Accepted version.
Published in *Inorganic Chemistry* **2020,** *59* (22), 16361-16374.
https://doi.org/10.1021/acs.inorgchem.0c02117

Theoretical description, synthesis, and structural characterization of β-$Na_{0.33}V_2O_5$ and its fluorinated derivative β-$Na_{0.33}V_2O_{4.67}F_{0.33}$: influence of oxygen substitution by fluorine on the electrochemical properties

Rafael Córdoba[a], Jakub Goclon[b,*], Alois Kuhn[a] and Flaviano García-Alvarado [a,*]

[a] *Universidad CEU San Pablo, Facultad de Farmacia, Departamento de Química y Bioquímica*

Urbanización Montepríncipe, 28668 Boadilla del Monte, Madrid, Spain. Universidad

[b] *Institute of Chemistry, University of Białystok, ul. K. Ciolkowskiego 1K, 15-245 Białystok (Poland).*

** corresponding authors*

Abstract

The structure of β-$Na_{0.33}V_2O_{4.66}F_{0.33}$ has been investigated by both theoretical and experimental methods. It exhibits the same structure as that of the parent bronze β-$Na_{0.33}V_2O_5$. The partial substitution of oxygen by fluorine has little effect on the average structure and cell parameters, but the sodium environment changes significantly. Using DFT calculations, we determined the most stable positions of fluorine atoms in the unit cell. It was found that the partial replacement of oxide by fluoride takes mainly place in the coordination sphere of Na producing a shortening of the Na-anion bond lengths. We also analyzed the electronic properties based on density of states and Bader charge distribution.

The crystallochemical situation of sodium ions in β-$Na_{0.33}V_2O_{4.67}F_{0.33}$ oxyfluoride, detected by both experimental and computational methods, affects its mobility with respect to the parent oxide. The

Accepted version.
Published in *Inorganic Chemistry* **2020,** *59* (22), 16361-16374.
https://doi.org/10.1021/acs.inorgchem.0c02117

higher ionicity in the Na coordination sphere of β-$Na_{0.33}V_2O_{4.67}F_{0.33}$ is related to a sodium ion diffusion coefficient, D_{Na+}, that is one order of magnitude lower (1.24×10^{-13} cm^2 s^{-1}) than in the case of β-$Na_{0.33}V_2O_5$ (1.13×10^{-12} cm^2 s^{-1}).

Electrochemical sodium insertion/deinsertion properties of the oxyfluoride have been also investigated and are compared to the oxide. Insertion/deinsertion equilibrium potential for the same formal oxidation state of vanadium increases due to fluorination (for instance reduction of $V^{+4.3}$ occurs at 1.5 V in the oxide and at 1.75 V in the oxyfluoride). However, the capacity of $Na_{0.33}V_2O_{4.67}F_{0.33}$ at constant current is lower than in the case of β-$Na_{0.33}V_2O_5$ due to a less adequate morphology, a lower D_{Na+}, and a lower oxidation state of vanadium owing to the aliovalent O/F substitution.

Introduction

Sodium-ion batteries are cost-effective alternatives to lithium-ion batteries. Despite its high abundance, sodium will replace lithium at large scales only if the specific energy significantly increases to compensate for the lower capacity usually reached with sodium hosts. Nonetheless and as for lithium-based systems, a 2-electron reversible processes would be desirable to alleviate the lower capacity of typical sodium hosts.[1] Vanadium compounds, owing to the variety of oxidation states of this metal, have attracted high interest and are becoming part of the state-of-the-art. Multielectron reversible processes have been successfully reached in polyanionic materials such as $VOPO_4$.[2] Song et al.[3] reported that monoclinic $NaVOPO_4$ is electrochemically active in the 2.0 – 4.4 V voltage range with deintercalation/intercalation of 1 Na. More recently, a multielectron process was enabled by previous insertion of sodium into $NaVOPO_4$. Thus, a specific capacity of 320 mAh g^{-1} was reported due to $V^{3+}/V^{4+}/V^{5+}$ redox couples in the 0.5-4.3 V voltage range.[4]

Accepted version.
Published in *Inorganic Chemistry* **2020,** *59* (22), 16361-16374.
https://doi.org/10.1021/acs.inorgchem.0c02117

Another way of improving the performance of electrode materials is to increase the voltage for a given redox couple by changing the transition metal ligands. Thus, for instance, substitution of oxygen by the more electronegative fluorine increases reduction potential. This effect is clearly seen when comparing the reduction potential of Ti^{4+}/Ti^{3+} in the oxide $Li_4Ti_5O_{12}$ (1.5 V vs. Li^+/Li)[5] with Li_2TiF_6 (2.8 V vs. Li^+/Li).[6] The topology and crystal chemistry of fluorides are different from those of oxides, making other redox couples available for reversible lithium intercalation. Thus, reversible lithium intercalation in vanadium oxides is frequently related to V^{5+}/V^{4+} and V^{4+}/V^{3+} redox couples. However, reversible lithium intercalation with reduction of V^{3+} to V^{2+} is not usual. Fluorides stabilize lower transition metal oxidation states, making these redox couples available. In such cases, stabilization of the lower oxidation state offsets the advantage of using the most electronegative ligand to increase the potential of cathode materials.

Increasing voltage while keeping the proper topology of oxide-type hosts and high oxidation states is possible by partial substitution of oxygen by fluorine in selected hosts. Such mixed-anion compounds, called oxyfluorides, are a part of a less explored chemistry if compared to oxides. An excellent overview on material chemistry and multiple anions has been recently published.[7] It has been pointed out that mixed anion chemistry gives new challenges to tune the electronic and atomic structure of materials and hence both chemical and physical properties. Thus, a variety of ligands available to replace the most common O^{2-} anion provide many interesting solids that challenge synthetic inorganic chemistry. Many success cases illustrate the variety of properties and types of compounds that mixed anions encompasse:[7] oxynitrides as photocatalytic materials or pigments, oxyfluorides and oxyhydrides as battery materials, oxychloride as pleochroic materials, etc. Several effects of mixed anions on electronic and atomic structures have been recently collected by Kageyama et al.[7] Among them, the indirect effect of anion substitution on the cation band relates to

Accepted version.
Published in *Inorganic Chemistry* **2020,** *59* (22), 16361-16374.
https://doi.org/10.1021/acs.inorgchem.0c02117

the aforementioned change of intercalation voltage. Therefore, energy storage materials can benefit from such a rich and unexplored chemistry in two ways: i) by providing new electroactive materials with modified topologies, connectivity or modified crystal field splitting, and ii) by increasing the redox potential. An interesting example of the former is layered $Na_5V(PO_4)_2F_2$.[8] It crystallizes in two different Space Groups. The dimorphs exhibit layered structures that can deintercalate/intercalate 1 Na^+/formula based on the oxidation/reduction of V^{3+} at ca. 3.5 V. Interestingly, the capacity retention is very high (over 1000 cycles) due to the very stable polyanionic framework. An example of the latter is $LiFeSO_4F$ [9] that exhibits a redox potential 750 mV higher than the homologous compounds $LiFePO_4$ or $Ag_2V_2O_6F_2$ [10] whose redox potential vs. Li^+/Li is 300 mV higher than for $Ag_2V_4O_{11}$.[11]

An interesting success case of mixed anion chemistry regarding the synthesis of new intercalation materials is VO_2F (space group R-3c). This is due to the high capacity it develops in lithium half-cells by multielectron processes.[12] It was synthetized for the first time in our group by solid state reaction at high temperature and high pressure and later on by mechanochemical reactions.[13, 14] VO_2F develops 263 mAh g^{-1} (1 Li^+/f.u.) in the 3.9 - 2.2 V vs. Li^+/Li voltage range, whereas a deeper discharge to 1 V provides a gravimetric capacity of 460 mAh g^{-1} (1.75 Li^+/f.u.). Interestingly, it exceeds that of the already commercialized $LiCoO_2$ and $LiFePO_4$ cathode materials. Unfortunately, according to our own unpublished results, the narrow tunnels left by the 3D-framework of VO_2F do not allow the intercalation of sodium, and an irreversible reduction of the oxyfluoride is observed instead.

On the other hand, there are several vanadium oxides that are able to insert sodium reversibly.[15-18] However, the one most investigated for lithium batteries, α-V_2O_5, shows no activity versus sodium unless tailored to nanosize. In this case, after an irreversible processes in the first cycle, it delivers a moderate capacity of 100 mAh g^{-1} upon discharge down to 1.8 V vs. Na^+/Na.[19]

Accepted version.
Published in *Inorganic Chemistry* **2020,** *59* (22), 16361-16374.
https://doi.org/10.1021/acs.inorgchem.0c02117

Conversely, the high pressure polymorph shows very interesting activity versus sodium, because it develops a capacity of 147 mAh g^{-1} in the 3.6 – 2 V range.[20] This capacity, corresponding to 1 Na^+/f.u., is quite limited when compared to lithium intercalation[21] (up to 2 Li^+/f.u.) and points to the different crystal chemistry that different guest ions display in the same hosts, as clearly evidenced for $A_2Ti_6O_{13}$ (A= H, Li or Na) compounds.[22-25]

In contrast to orthorhombic layered α-V_2O_5 (S.G. *Pmmn*),[26, 27]sodium vanadium bronze β-$Na_{0.33}V_2O_5$ with the β-type structure crystallizes in the monoclinic system (S.G.*A2/m*) within the range $Na_{0.22}V_2O_5$-$Na_{0.4}V_2O_5$.[28] Fig. 1a shows a schematic representation of the structure of β-$Na_{0.33}V_2O_5$. The structure consists of zigzag double chains of [V-O_6] octahedra that form sheets by joining corners. These sheets are separated by additional chains of double [V-O_5] square pyramids, giving rise to unidirectional tunnels along the *b* axis in which the Na ions are located.

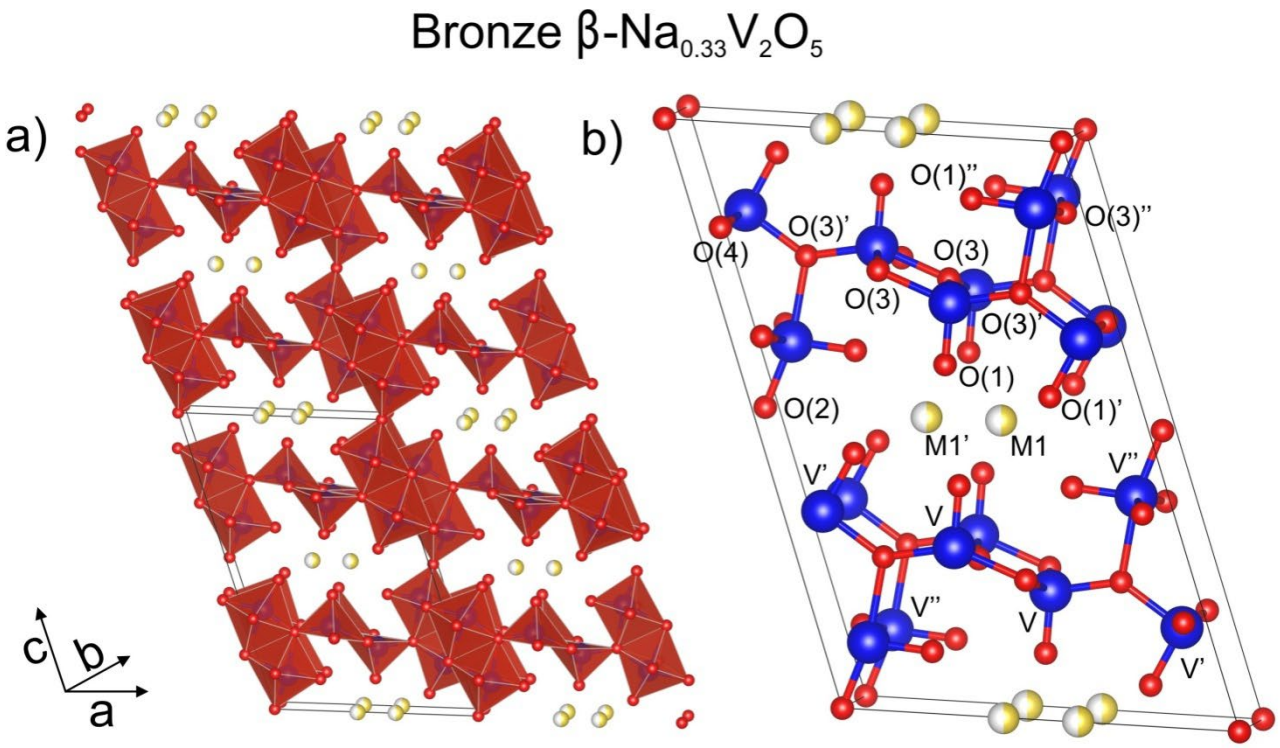

Accepted version.
Published in *Inorganic Chemistry* **2020,** *59* (22), 16361-16374.
https://doi.org/10.1021/acs.inorgchem.0c02117

Figure 1. a) Side view of the bronze β-$Na_{0.33}V_2O_5$ structure (with unit cell indicated). b) Different types of vanadium, oxygen and sodium centers are shown. The V, O, and Na atoms are shown as blue, red, and white-yellow spheres, respectively.

The V-O arrangement forming the above described three-dimensional framework with tunnels along the direction [010] is able to allocate different alkali and other monovalent and divalent metals in some other different sites (M1/M1' c.n.= 7, M2/M2' c.n.= 8 and M3/M3' c.n.= 4).[28, 29] In the case of sodium, it half fills M1/M1' for the composition $Na_{0.33}V_2O_5$. Full occupancy of M1/M' positions would produce too short Na-Na distances. Thus, although full occupancy of the three positions above mentioned by Na would produce the composition $Na_2V_2O_5$, this composition seems to be difficult to reach. The first reports on Na intercalation claimed that 1.33 sodium atoms are inserted[30] in the 3.5 - 1.0 V vs Na^+/Na voltage range. Later on, Bach et al.[31] investigated the insertion of sodium in the 3.4 - 2.4 V vs. Na^+/Na voltage range for two different samples, one prepared by solid state reaction and the other by a sol-gel route. For the latter, the electrochemical insertion of sodium giving $Na_{0.33+x}V_2O_5$ phases proved to be reversible reaching x = 0.66 (that would correspond to half filling of M1/M1', M2/M2´, and M3/M3´ for NaV_2O_5).[31] Interestingly, the authors claimed that "*structural anisotropy*" provided by the sol-gel route is the origin of the better electrochemical behavior if compared with the sample prepared by ceramic route.

Regarding sodium extraction from β-$Na_{0.33}V_2O_5$, Pereira-Ramos et al. reported that Na could not be extracted from samples prepared by a sol-gel process.[32] However, a more recent report claims that when the bronze is prepared by a ceramic, chemical switch route, extraction of sodium is possible.[33] Interestingly, the extraction of Cu from β-$Cu_{0.55}V_2O_5$ produces the β´-V_2O_5 polymorph.[34]

Accepted version.
Published in *Inorganic Chemistry* **2020,** *59* (22), 16361-16374.
https://doi.org/10.1021/acs.inorgchem.0c02117

This demonstrated that β´-V_2O_5 is stable and that reversible insertion of 1 sodium may produce a very interesting sodium cathode by analogy with lithium.[34]

We are presently addressing the synthesis and electrochemical characterization of new oxyfluorides as sodium intercalation hosts. Also, having in mind possible 2-*electron* hosts, vanadium oxides are attractive candidates for substitution of oxygen by fluorine.

Partial replacement of oxygen by fluorine could enable an increase in the insertion voltage of $Na_{0.33}V_2O_5$. Galy *et al.*[35] reported the existence of a solid solution with the composition $Na_xV_2O_{5-x}F_x$ (x = 0.18 - 0.33) with the β-bronze structure. Looking for the maximum effect that substitution of oxygen by fluorine may have on the electrochemical properties, we have investigated the member x = 0.33. In the present work, we investigate the effect of fluorination on the β-$Na_{0.33}V_2O_5$ structure using computational and diffraction methods, as well as on its electrochemical properties.

Insight into the β- $Na_{0.33}V_2O_5$ bronze structure

The elementary unit cell contains 44 atoms (6 stoichiometric units of V_2O_5 and 2 Na atoms), as shown in Fig. 1b. The lattice parameters are *a* = 10.08 Å, *b* = 3.61 Å, *c* = 15.41 Å and *β*= 109.5º. At a sodium stoichiometry of 0.33, there are exactly two sodium atoms per primitive cell. In this structure, the sodium ions can occupy two closely spaced tunnel positions labelled M1 and M1', see Fig. 1b. However, simultaneous full occupation of the two sites is not possible because of the short interionic distance (~1.90 Å). This situation is similar to that found for sodium intercalated TiO_2 hollandite.[36]

In the crystal structure, vanadyl oxygen atoms, denoted as O(1) and O(1)' (see Fig. 1b) are bound to V and V' by a double bond (along the *c* direction) with the distances equal to 1.56 and 1.66

Accepted version.
Published in *Inorganic Chemistry* **2020,** *59* (22), 16361-16374.
https://doi.org/10.1021/acs.inorgchem.0c02117

Å, respectively. The vanadyl oxygen atoms oriented along the *a* direction that form bonds of 1.63 Å with V'' atoms are denoted as O(1)''. The bridging oxygen atom O(2) connects two V'' atoms along the **c** direction with equal bond distances of 1.79 Å. Threefold-coordinated oxygen atoms, denoted as O(3), have two shorter (1.88 Å) bonds and one longer (1.98 Å) bond with V atoms along the **b** direction. These are denoted as O(3)' and form bonds with V, V', and V'' atoms equal to 1.80, 1.91, and 2.18 Å, respectively. Whereas these denoted as O(3)'' form two short (1.88 Å) bonds with V'' atoms and one longer (2.03 Å) bond with V' atoms along the *b* direction. Fourfold-coordinated oxygen atoms, denoted as O(4), have two shorter (1.86 Å) bonds with V atoms and two longer bonds with V' (2.41 Å) and V'' (2.33 Å). Every vanadium atom is coordinated to either five (V) or six (V' and V'') oxygen atoms. As a result, eight distinct oxygen and three vanadium atom types can be distinguished in the bronze β-$Na_{0.33}V_2O_5$ bulk structure. Each of them exhibits different chemical properties.

Methods

Computational details

All of the calculations were performed at the DFT level using the Perdew-Burke-Ernzerhof (PBE) generalized-gradient approximation[37] to the exchange-correlation function as implemented in the PWscf[38] code. The interaction between the ions and the valence electrons is described by Vanderbilt ultrasoft pseudopotentials.[39] A plane-wave cutoff of 50 Ry was chosen for these calculations, while the charge density cutoff was set to 500 Ry. To improve the description of the long range nonlocal correlation effects, which play a crucial role in weak interacting systems such as β-$Na_{0.33}V_2O_5$, we employed one of the van der Waals semi-empirical dispersion correction (D3) proposed by S. Grimme.[40] This approach (DFT-D3) consists of adding a semiempirical dispersion potential (a pairwise force field including two terms) to the Kohn-Sham DFT energy. In addition, for

Accepted version.
Published in *Inorganic Chemistry* **2020,** *59* (22), 16361-16374.
https://doi.org/10.1021/acs.inorgchem.0c02117

a better description of the electronic structure of Bronze β-$Na_{0.33}V_2O_5$, we applied the DFT+U method,[41, 42] which allows us to adjust the position of V 3*d* electron levels results in the improvement of the band gap energy. In the present work, we adopted the DFT + U formulation by Dudarev et al.[43] as implemented by Cococcioni and de Gironcoli.[44] A 6 x 12 x 4 Monkhorst-Pack[45] mesh was used to integrate the Brillouin zone. The total energy was minimized using the Hellman–Feynman forces. The examined systems were fully relaxed until the residual forces on the ions were below 2.5×10^{-3} eV $Å^{-1}$. All the calculations were spin polarized.

To calculate the total and projected density of states (DOS), linear tetrahedron smearing was used. The peak width for broadening was set to 0.05 eV for a better visualization of the plot of the DOS. The Bader charges[46] were calculated using the Bader program[47] for the single point self-consistent-field calculations of the previously optimized structures using the projector-augmented-wave (PAW) pseudopotentials[48] with 100 Ry and 1000 Ry kinetic energy cut-off for the wave-functions and charge densities, respectively.

For some V_2O_5 systems, the band gap is correctly estimated for higher values of U, but it also depends on the applied DFT+U scheme. Note that the position of V 3d electron levels needs to be adjusted by changing the U value, since the standard DFT methods underestimate the band gap by 30-40%. This issue was comprehensively discussed by Jovanović et al.[49] The authors used U_{eff} = 6 eV (the Dudarev et al.[43] scheme with the Grimme correction (D2) using Vanderbilt ultrasoft pseudopotentials included in the PWscf program) for the proper description of the electronic properties of α-V_2O_5; therefore, we also decided to take this value for the description of our systems due to the lack of the proper experimental data.

Accepted version.
Published in *Inorganic Chemistry* **2020,** *59* (22), 16361-16374.
https://doi.org/10.1021/acs.inorgchem.0c02117

All structures and atomic arrangements were prepared by using VESTA[50] and XcrySDen[51] programs.

Synthesis

The synthesis of β-$Na_{0.33}V_2O_5$ was carried out following the procedure described by Mukainakano *et al*.[52] Reactants (NaOH and NH_4VO_3 at a 1:6 molar ratio, both from Sigma-Aldrich) were heated at 600 ºC for 5 hours under Ar atmosphere, in a tubular furnace, using a 10 ºC/min heating rate. On the other hand, a fluorinated derivative with the nominal composition β-$Na_{0.33}V_2O_{4.67}F_{0.33}$ was synthetized by a similar ceramic method in which NaF was used as the source of both sodium and fluoride ions.[35] A mixture of NaF, VO_2, and V_2O_5 (Sigma-Aldrich) in stoichiometric amounts according to the following reaction

$0.33\ NaF + 0.66\ VO_2 + 0.66\ V_2O_5 \rightarrow Na_{0.33}V_2O_{4.67}F_{0.33}$

was ground and pressed into pellets. They were placed into a copper tube, sealed under Ar atmosphere, heated at 450 ºC for 12 hours, and allowed to cool. The as-obtained product was ground, newly pressed, and heated again under the same conditions.

Removal of sodium from both oxide and oxyfluoride was tried by two different methods:

i) Chemical oxidation using NO_2BF_4 as oxidizing agent following the procedure detailed in ref.[34] Approximately 200 mg of these compounds in a solution of acetonitrile containing 25% excess of NO_2BF_4 as the oxidizing agent were stirred and heated under reflux for 24 hours. Once the reaction was finished, the resulting compound was repeatedly washed with acetonitrile and finally dried. The whole oxidation process was repeated twice in order to extract the maximum possible sodium amount.

ii) Electrochemical oxidation. These experiments were performed in Swagelok™ type cells, using metallic sodium as the anode, stacked with a glass fiber paper separator and a 1M $NaClO_4$ 1:1 solution

Accepted version.
Published in *Inorganic Chemistry* **2020,** *59* (22), 16361-16374.
https://doi.org/10.1021/acs.inorgchem.0c02117

of ethylene carbonate (EC) and propylene carbonate (PC) as the electrolyte. The positive electrode consisted of a composite of the active material (sodium vanadium oxide or oxyfluoride), Super P Timcal conductive carbon, and PVDF as binder in a 85:10:5 weight ratio. Cells were charged in potentiostatic mode to 4.2 V vs. Na^+/Na and kept at that voltage until the current decayed by four orders of magnitude (referred to the initial current peak). Afterwards, the electrodes were removed from the electrochemical cell and washed with EC and N-methyl pyrrolidone (NMP) for further characterizations. However, due to incomplete oxidation, none of the oxidized samples were finally used for further characterization.

Structural and chemical characterization

The phase purity and structures of both the oxide and oxyfluoride were studied by powder X-ray diffraction (PXRD). $Na_{0.33}V_2O_5$ bronze was measured in an X'pert PRO ALPHA 1 model PANalytical diffractometer in transmission geometry using 0.5 mm rotating capillaries to avoid surface preferred orientation, which is a commonly observed phenomenon for crystals exhibiting acicular morphology when mounting samples on a flat-plate in Bragg-Brentano geometry. $Na_{0.33}V_2O_{4.67}F_{0.33}$ was measured by means of a Bruker D8 high-resolution diffractometer equipped with a solid-state position sensitive rapid LynxEye® detector (PSD), using CuKα radiation ($\lambda_{\alpha 1}$ =1.5406 Å, $\lambda_{\alpha 2}$ = 1.54439 Å). Morphology of both compounds was studied by means of Scanning Electron Microscopy, using a JEOL JSM-6400 microscope; while sodium content was determined by using Energy-dispersive X-ray Spectroscopy (EDS) carried out in a JEOL JSM-2100 microscope. In order to determine the fluorine and oxygen contents in β-$Na_{0.33}V_2O_{4.66}F_{0.33}$, Wavelength-dispersive Spectroscopy (WDS) was used in a JEOL Superprobe JXA-8900M microscope.

Electrochemical characterization

Accepted version.
Published in *Inorganic Chemistry* **2020,** *59* (22), 16361-16374.
https://doi.org/10.1021/acs.inorgchem.0c02117

Electrochemical experiments were performed in CR2032 coin cells assembled in an argon atmosphere. Their configuration was the same as that described for the Swagelok™ type cells. Near-equilibrium experiments were performed down to two different lower cut-off voltages (2 and 1 V vs. Na^+/Na, respectively) using the galvanostatic intermittent titration technique (GITT). A current of 107.2 µA was applied for 60 min to reach a 0.05 incremental change of sodium content, after which the cell was allowed to relax for 8 h. Galvanostatic discharge-charge experiments were carried out at a C/20 rate (i.e., the current required to insert 1 Na atom in 20 hours was applied) from OCV down to either 1 V or 2 V vs. Na^+/Na.

For determination of the sodium diffusion coefficient, Impedance Spectroscopy was used to obtain the Warburg coefficient, while BET experiments (Micromeritics ASAP 2020 analyzer) provided the electrode specific area, A. Impedance measurements were carried out in three-electrode cells at OCV conditions. Sodium disks were placed at both counter and reference electrodes, whereas either β-$Na_{0.33}V_2O_5$ or β-$Na_{0.33}V_2O_{4.66}F_{0.33}$ was used as the electroactive component of the positive electrode. An AC perturbance of 10 mV was applied while the impedance was recorded in the frequency range of 1 MHz - 1 mHz. Equivalent circuit modelling was made using the Z-Fit (EC-lab® software).

Results and discussion

Analysis of the X-ray diffraction patterns of samples with nominal content β-$Na_{0.33}V_2O_5$and β-$Na_{0.33}V_2O_{4.66}F_{0.33}$, synthesized as described above, indicate that reflections can be indexed with the unit cell as described by Wadsley[28] and Galy[35], respectively. EDS spectra taken from crystals showing electron diffraction patterns characteristic of the monoclinic cell of β-$Na_{0.33}V_2O_5$ indicate the presence of fluorine in the oxyfluoride. The O/F ratio of 11.5, determined by WDS, agrees fairly well with that expected for the nominal composition $NaV_6O_{14}F$. This demonstrates the partial

Accepted version.
Published in *Inorganic Chemistry* **2020,** *59* (22), 16361-16374.
https://doi.org/10.1021/acs.inorgchem.0c02117

fluorination of β-$Na_{0.33}V_2O_5$. Estimated compositions correspond to β-$Na_{0.29(1)}V_2O_5$ and β-$Na_{0.34(1)}V_2O_{4.67(13)}F_{0.40(1)}$ which are close to the nominal ones. For the sake of clarity, we will refer to them throughout this report using nominal compositions or the names *oxide* and *oxyfluoride*, respectively.

X-ray diffraction and morphology

The influence of fluorine in the crystal structure of the pristine bronze has been investigated by Rietveld analysis. However, due to the similar X-ray scattering factors of O and F, the analysis of structural differences was also addressed by theoretical methods. The X-ray diffraction patterns of pristine β-$Na_{0.33}V_2O_5$ and β-$Na_{0.33}V_2O_{4.67}F_{0.33}$ (Fig. 2a) were fully indexed with space group *A2/m*, in agreement with previous works.[28, 33] A small amount of VO_2 (rutile, S.G. $P2_1/c$) as a minor secondary phase (4.6%) in β-$Na_{0.33}V_2O_{4.67}F_{0.33}$ was included in refinements.

Fig. 2b shows SEM images corresponding to β-$Na_{0.33}V_2O_5$ and β-$Na_{0.33}V_2O_{4.67}F_{0.33}$. The former exhibits stick like morphology with a length ranging from 2 to 6 μm and a width of approximately 1 μm. By contrast, the latter exhibits a very different morphology. It shows quite heterogeneous sizes ranging from small rounded shaped crystals of 1 μm, and even smaller, to big chunks of more than 7 μm.

For β-$Na_{0.33}V_2O_5$, the refined lattice parameters are a = 10.0815(1) Å, b = 3.61300(4) Å, c = 15.4382(2) Å and β = 109.5681(7)º, which are consistent with previous reports[19]. Likewise, the refined lattice parameters for β-$Na_{0.33}V_2O_{4.67}F_{0.33}$ are a = 10.1333(4) Å, b = 3.6208(1) Å, c = 15.4555(7) Å, and β = 109.104(3)º, which were in very good agreement with literature[26]. Tables S1 and S2 of the SI show the atomic positions, thermal displacement factors, and occupancies for $Na_{0.33}V_2O_5$ and $Na_{0.33}V_2O_{4.67}F_{0.33}$ obtained after Rietveld refinement from XRD data. Experimental data listed in Table

Accepted version.
Published in *Inorganic Chemistry* **2020,** *59* (22), 16361-16374.
https://doi.org/10.1021/acs.inorgchem.0c02117

1 point to a small increase of the cell volume (~ 1%) upon partial replacement of oxide ions, even though the fluoride ion is supposed to be smaller for the same coordination number.

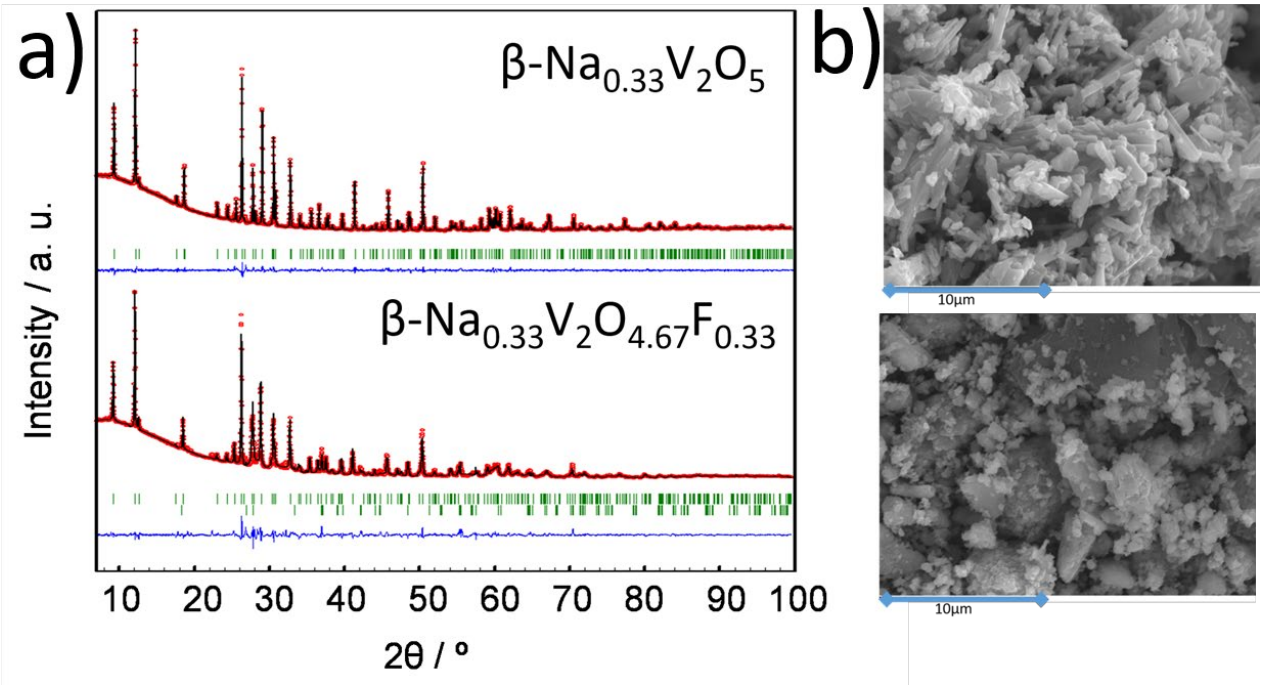

Figure 2. a) Experimental (red points), calculated (solid black line) XRD patterns and their differences (blue line at bottom) for β-$Na_{0.33}V_2O_5$ and β-$Na_{0.33}V_2O_{4.67}F_{0.33}$. The vertical bars indicate the positions of the Bragg peaks. b) SEM images showing the different morphology of β-$Na_{0.33}V_2O_5$ (top) and β-$Na_{0.33}V_2O_{4.67}F_{0.33}$ (bottom).

Due to the similar scattering factor of O and F, reliable structure determination can be done only if both anions are very well ordered. However, the analysis of formal valences and bond distances gives valuable information.

To assess the formal valences of the three types of vanadium atoms (V1, V2 and V3) in both oxide and oxyfluoride compounds, we applied the valence bond (VB) approach.[53, 54]

Accepted version.
Published in *Inorganic Chemistry* **2020,** *59* (22), 16361-16374.
https://doi.org/10.1021/acs.inorgchem.0c02117

Interatomic distances from the structural models refined from powder X-ray diffraction for $Na_{0.33}V_2O_5$ have been used in the valence bond calculations.

The conventional R_0 value of 1.803 for V^{5+} has been used.[53, 54] The valences of the three V atoms in $Na_{0.33}V_2O_5$ were calculated as follows: V1 = 4.842+, V2 = 4.771+ and V3 = 4.880+. The value of the mean valence of all three V atoms in our analysis, 4.831+, is in excellent agreement with the formal oxidation state derived from nominal composition $(Na^+)_{0.33}(V^{4.835+})_2O_5$, in which the extra electrons are supposed to be equally distributed among all three V atoms.

Table 1: Crystallographic data of $Na_{0.33}V_2O_5$ and $Na_{0.33}V_2O_{4.67}F_{0.33}$ compounds obtained from XRD data and from computational methods.

	$Na_{0.33}V_2O_5$		**$Na_{0.33}V_2O_{4.67}F_{0.33}$**	
	Experimental (XRD)	Computational (DFT)	Experimental (XRD)	Computational (DFT)
a (Å)	10.0815(1)	10.06	10.1333(4)	10.13
b (Å)	3.61300(4)	3.66	3.6208(1)	3.69
c (Å)	15.4382(2)	15.33	15.4555(7)	15.14
β(º)	109.5681(7)	109.60	109.104(3)	109.37
Vol ($Å^3$)	529.85(1)	531.739	535.84(3)	534.967

For comparison, we calculated valences for the same compound using the crystallographic data reported by Khamaganova &Trunov[55] yielding V1: 4.916+, V2: 4.924+; V3: 4.926+. Though these values are in fair agreement with our results, they systematically overestimate

Accepted version.
Published in *Inorganic Chemistry* **2020,** *59* (22), 16361-16374.
https://doi.org/10.1021/acs.inorgchem.0c02117

the valence of vanadium. On the other hand, our values were also systematically lower than those reported by Streltsov for the bronze $Cu_{0.63}V_2O_5$[56] which not only differ in the amount of monovalent tunnel ion but also with regard to the Na and Cu positions. Nevertheless, in agreement with Streltsov, the lowest valence is obtained for the V2 atom, which appears to be the vanadium ion with the highest charge from multipole analysis of the electron density in $Na_{0.33}V_2O_5$[57] and, furthermore, has been proposed to be strongly involved in the charge ordering in this sodium vanadium oxide bronze.[58]

The valence bond analysis of the three V atoms performed in $Na_{0.33}V_2O_{4.67}F_{0.33}$ oxyfluoride resulted in the following: V1 = 4.482+, V2 = 4.750+, and V3 = 4.759+, with a mean valence of 4.664+ for all three V atoms. Again, the mean valence of all three V atoms in our bond valence analysis is in excellent agreement with the formal oxidation state derived from its nominal composition $(Na^+)_{0.33}(V^{4.67+})_2O_{4.67}F_{0.33}$. We must note that these values are systematically lower than those calculated in $Na_{0.33}V_2O_5$, in accordance with the underlying substitution mechanism, after which the charge compensation for substituting one O^{2-} with 1 F^- is accompanied by simultaneous reduction of one V^{5+} to V^{4+}. The decrease in valence appears to be more pronounced for V1 (-7.4%) and V3 (-2.5%) when compared to V2 (-0.4%).

One may now hypothesize that V atoms statistically surrounded with more F atoms will undergo a stronger decrease of their valences, which appear to be V1 and V3, while the valence of V2 remains almost unchanged and thus seems to exhibit a surrounding that mainly consists of oxygen atoms. Concerning the environment of the channel ion, we note that every Na^+ ion is hepta-coordinated with O/F anions in a distorted capped trigonal prism configuration, sharing square faces with a neighbor equivalent $Na(O/F)_7$ polyhedron along the *a* direction. These double capped trigonal prisms further share their trigonal faces along the channel *b* direction. Interestingly, the average Na-O/F bond lengths in $Na_{0.33}V_2O_5$ oxide, 2.511 Å, decrease to 2.483 Å upon doping with fluorine in

Accepted version.
Published in *Inorganic Chemistry* **2020,** *59* (22), 16361-16374.
https://doi.org/10.1021/acs.inorgchem.0c02117

$Na_{0.33}V_2O_{4.67}F_{0.33}$ oxyfluoride (Fig. S1 of SI). The shortening of the Na-anion bond length in sodium vanadium oxyfluoride points to Na^+ surrounded with both F and O atoms, owing to the smaller size of F^-.[59] To summarize, Na ions in the oxyfluoride present shorter sodium-anion bond lengths and a more fluoride-rich environment at the same time. This different crystallochemical situation could affect the mobility of Na ions in $Na_{0.33}V_2O_{4.67}F_{0.33}$ oxyfluoride.

In any case, it should not be forgotten that the application of the VB method may only be of limited use in systems with strongly distorted V-O polyhedra and highly correlated electrons, where strong electron interactions determine the type of ground state of the cation. Therefore, the ligand environment of Na has been also analyzed by computational methods. Note that DFT has been proven to be particularly useful for the analysis of anion distribution in mixed anion compounds.[7]

Theoretical analysis

The optimization of the unit cell shape of the bronze β-$Na_{0.33}V_2O_5$ with the internal atomic coordinates was performed using variable-cell calculations. The whole procedure was repeated a few times, always using all parameters obtained from the previous run to get better convergence. The optimized equilibrium lattice constants (a = 10.06 Å, b = 3.66 Å, c = 15.33 Å with β = 109.60^o) are in excellent agreement with the experimental data (See Table 1). Note that the experimental data have been fitted using the nomenclature corresponding to the different crystallographic positions in S.G. *A2/m*. Since the introduction of F atoms into the primitive unit cell removes the symmetry of all atoms, different nomenclature for both atoms was thus applied (see Figure 1b). The error for a parameter is 0.2%, for b is 1.4% and for c is 0.7%. The computational setting used, including the on-site coulombic interaction of the V *3d* states combined with van der Waals dispersion corrections, has been commonly applied for the description of different doped vanadium pentoxide systems.[49, 60-62]

Accepted version.
Published in *Inorganic Chemistry* **2020,** *59* (22), 16361-16374.
https://doi.org/10.1021/acs.inorgchem.0c02117

The simulation cell contains two V_2O_5 layers along the *c* direction. The Na ions are in the middle of [V-O_5] pyramids and between every layer (M1 sites), see Fig. 3a**.** After the geometry optimization, the oxygen atoms around the Na ion form a polyhedron with eight faces, see Fig. 3b. The corresponding distances between Na and O(1) (from the top layer), O(1)', O(1) (from the bottom layer) and O(1)'' are 2.63, 2.48, 2.47, and 2.35 Å, respectively**.** The previously described vanadium-oxygen distances are slightly more differentiated. However, we concentrated only on the bond changes in the close vicinity of the Na ion for transparency. Lattice constants and internal positions of atom centers inside the optimized unit cell of the bronze β-$Na_{0.33}V_2O_5$ are gathered in Table S4 of the SI.

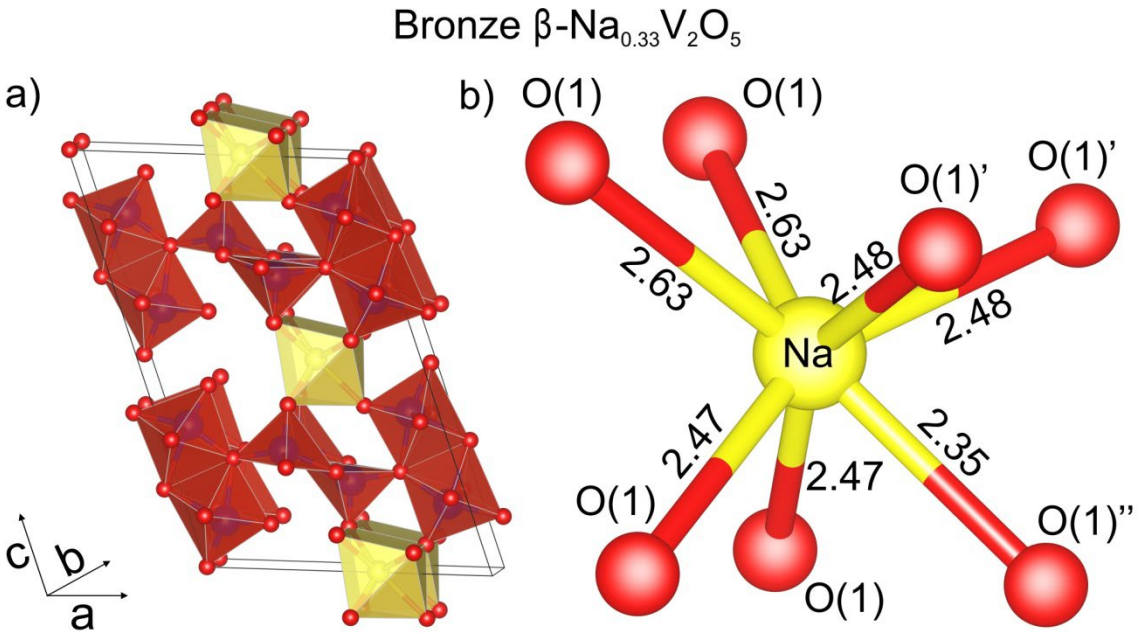

Figure 3. a) Side view of the DFT(PBE+U)+D3-optimised structure of the Bronze β-$Na_{0.33}V_2O_5$ bulk unit cell. b) Different types of oxygen centers are shown. The bonds of interest are displayed (in Å). The V, O, and Na atoms are shown as blue, red, and yellow spheres, respectively.

Accepted version.
Published in *Inorganic Chemistry* **2020,** *59* (22), 16361-16374.
https://doi.org/10.1021/acs.inorgchem.0c02117

To analyze the binding interaction between Na and the V-O framework, we studied first the electronic properties of β-$Na_{0.33}V_2O_5$. As seen in Fig. 4a, the DOS plot of β-$Na_{0.33}V_2O_5$ indicates a half-metallic behavior. The appearance of the partially occupied band has been also reported for the metal-doped α-V_2O_5 system.[49] Bronze β-$Na_{0.33}V_2O_5$ shows that the Na 3s states are mixed with the V and O states over the whole range of the valence band (VB). It is characterized as a mixture of O 2p and V 3d orbitals mainly in the bottom and middle part. States originating from the O 2p dominate in the top part of VB, while the contribution from V 3d is largest in the higher conduction bands (with a negligible contribution of oxygen states).

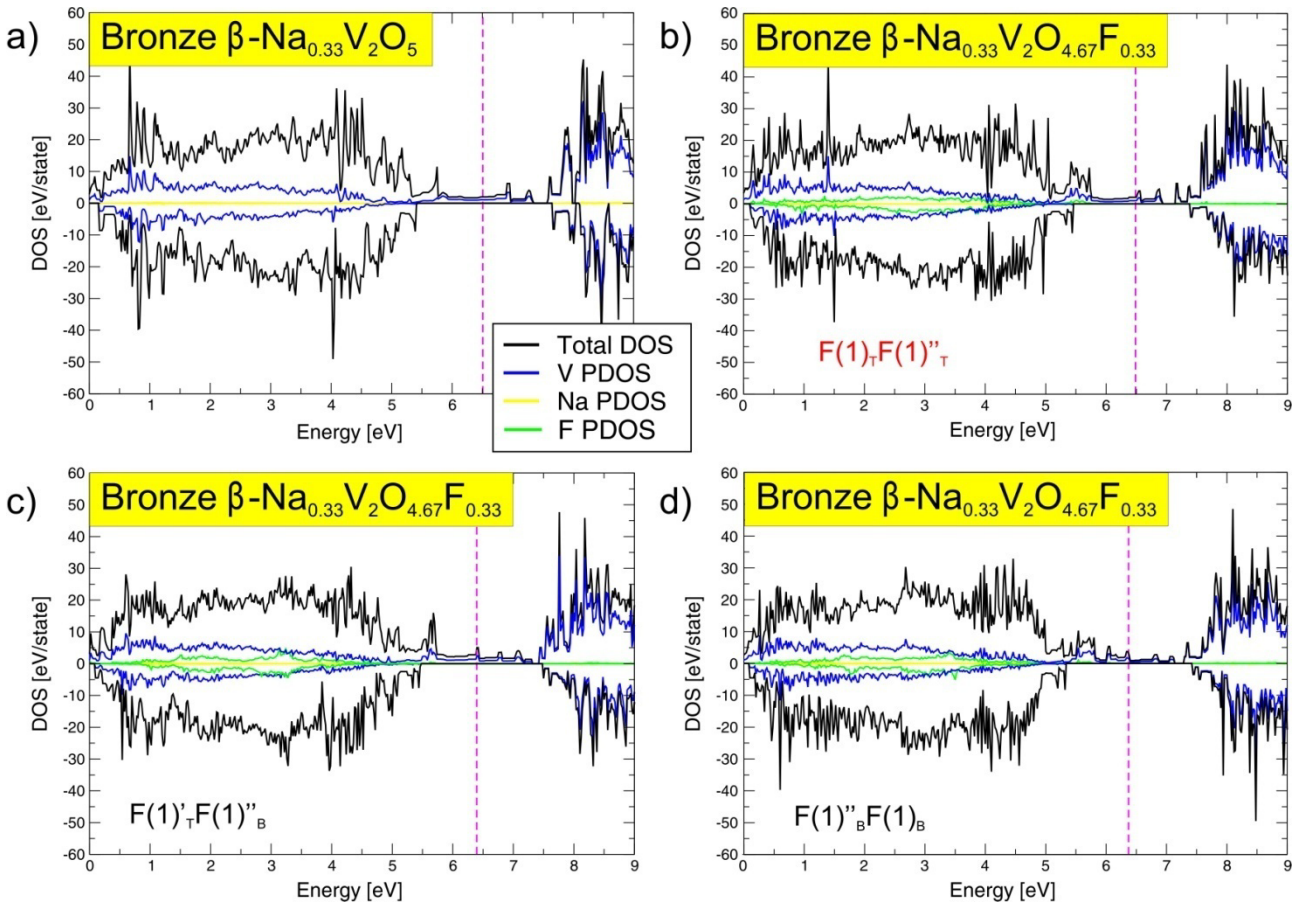

Figure 4. Total and projected density of states (DOS) obtained from the DFT(PBE+U)+D3 calculations for Bronze β-$Na_{0.33}V_2O_5$ (a) and the three most stable configurations of Bronze β-$Na_{0.33}V_2O_{4.67}F_{0.33}$ (b-d). The Fermi level is marked by the dashed pink line.

Accepted version.
Published in *Inorganic Chemistry* **2020,** *59* (22), 16361-16374.
https://doi.org/10.1021/acs.inorgchem.0c02117

Na ions and relaxation influence the oxidation state of all atoms. In the sodium-free β-V_2O_5, the formal oxidation state of vanadium is five and of oxygen is two. The presence of sodium slightly changes the vanadium state. Hence, the geometry relaxation leads to a distribution of the excess charge created by Na ions over the neighboring oxygen atoms. The Bader charge analysis indicates that about 0.90e^- per one Na was transferred. In this section, only the atomic charges of oxygen atoms in the close vicinity of the Na ion are presented for clarity. The lowest values of the oxidation states of oxygen are -0.72/-0.76, -0.84 and -0.83 for $O(1)_T/O(1)_B$, $O(1)'_T$ and $O(1)''_B$ (T - top layer, B - bottom layer), respectively. While the highest value was for the O(4) atom, and it is equal to -1.14. The calculated oxidation states for V atoms are in the range 2.14 – 2.24. It is thus seen that the oxidation states obtained for vanadium and oxygen atoms are strictly lower than the formal ones.

Next, we established the most stable configurations of bronze β-$Na_{0.33}V_2O_{4.67}F_{0.33.}$ This part of study is pivotal for a complete understanding of the influence of fluorine not only on the structural and electronic properties of Bronze β-$Na_{0.33}V_2O_5$ but also on the electrochemical performance. Geometry optimizations were performed for more than 20 initial configurations with fluorine atoms. In the unit cell, two O atoms were replaced by two F atoms according to the stoichiometry. Initially, we considered different types of combinations. However, the most stable structures were found for those with the fluorine atoms in the positions of vanadyl oxygen atoms (O(1), O(1)', and O(1)''). In Fig. 5, we present such configurations. Interestingly, these are the ligands which coordinate the position of sodium ion. In addition, we also included two less stable configurations with fluorine in the positions of O3 and O3' oxygen atoms for comparison.

For clarity, all configurations are named according to the positions of two inserted fluorine atoms instead of oxygen ones. The abbreviation $F(n)_PF(m)_{P'}$ refers to the combinations of two oxygen

Accepted version.
Published in *Inorganic Chemistry* **2020,** *59* (22), 16361-16374.
https://doi.org/10.1021/acs.inorgchem.0c02117

sites (n, m) and their positions (P, P') in the bulk unit cell including two layers, namely, the top (T) and bottom (B) ones, see Fig. 5 .

With the DFT(PBE+U)+D3 approach, we obtained bulk lattice parameters of *a* = 10.13 Å, *b* = 3.69 Å, *c* = 15.14 Å, and with *β* = 109.37° for the bronze β-$Na_{0.33}V_2O_{4.67}F_{0.33}$. These values agree well with the experimental data (*a* = 10.13 Å, *b* = 3.62 Å, *c* = 15.46 Å, and with *β* = 109.10°) (See Table 1). The *a* value is the same as the experimental value, the *c* value is smaller than the experimental one by 2.1%, while the *b* value is larger by 1.9%. The discrepancy between the calculated and the experimental length of the lattice vector *c* was found to be 0.32 Å. In the experiment, we obtained a mean value of the vector *c* associated with randomly distributed fluorine atoms in the bulk, whereas the optimization procedure was applied only to one structure, namely $F(1)_TF(1)'_T$. However, our test calculations for a few selected configurations show that the changes obtained for the lattice parameters have a marginal influence on the total energy.

Now, we discuss the results of the investigation of different insertion patterns of fluorine atoms into the bronze β-$Na_{0.33}V_2O_5$ bulk structure. The most stable configuration is $F(1)_TF(1)''_T$ with the total energy value (E_{rel}) set to 0 meV as the reference energy. In this structure, the Na ion was initially set in position M1; however, after the geometry optimization it moved to position M1'. The similar structure that is less stable by 72 meV is $F(1)''_BF(1)_B$ which differs only in the location of the Na ion (M1). A slightly less stable structure with an E_{rel} of 75 meV is structure $F(1)'_TF(1)''_B$. These three most stable configurations show the same characteristic pattern, namely, the F atoms introduced formed a triangle as one of the polyhedron's faces around the Na ion, see Fig. 5. For all other cases with fluorine atoms in different positions of vanadyl oxygen atoms, the values of an E_{rel} are contained in the range of 109 - 303 meV. Finally, the insertion of one and two F atoms in the position of the three-fold coordinated O atoms leads to less stable systems with the E_{rel} of 591 and 1634 meV,

Accepted version.
Published in *Inorganic Chemistry* **2020,** *59* (22), 16361-16374.
https://doi.org/10.1021/acs.inorgchem.0c02117

respectively. It is thus clear that the inserted fluorine atoms in bronze β-$Na_{0.33}V_2O_{4.67}F_{0.33}$ should mainly occupy the one-fold coordinated oxygen sites.

Now, we compare the geometric and electronic differences between the three most stable configurations (all coordinates are listed in Table S5 of the SI). For the $F(1)_TF(1)''_T$ configuration, the $F(1)''_T$ – Na and $F(1)_T$ – Na distances are 2.30 and 2.45 Å, respectively. The calculated equilibrium $F(1)''_B$ – $Na/F(1)_B$ – Na and $F(1)'_T$ – $Na/F(1)''_B$ – Na bonds in $F(1)''_BF(1)_B$ and $F(1)'_TF(1)''_B$ are 2.26/2.32 and 2.35/2.22 Å, respectively. By contrast, the distances between the Na ions and different vanadyl oxygen atoms are larger and contained in the range from 2.53 to 2.82 Å for all three cases. On the other hand, the different vanadium-fluorine bond lengths vary from 1.89 to 1.94 Å, while the changes that appeared in all vanadium-1-fold coordinated oxygen distances never exceeded 0.02 Å compared to the undoped bronze β-$Na_{0.33}V_2O_5$ bulk (1.60 - 1.62 Å). In all three cases, the oxidation states of vanadium atoms forming bonds with fluorine atoms are in the range 2.06 - 2.26 e, and they are only slightly lower than those for the undoped systems (2.14 - 2.24 e). All changes in the oxygen charges are less than 0.15 e, while the Bader charges on Na ions do not change.

Accepted version.
Published in *Inorganic Chemistry* **2020,** *59* (22), 16361-16374.
https://doi.org/10.1021/acs.inorgchem.0c02117

$F(1)_TF(1)'_T$ 303

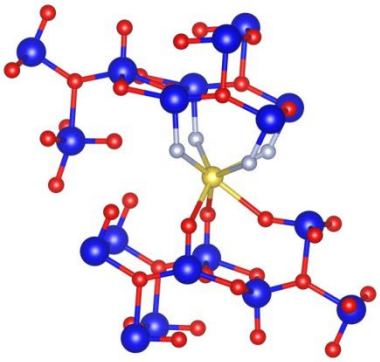

$F(1)_TF(1)''_B$ 211

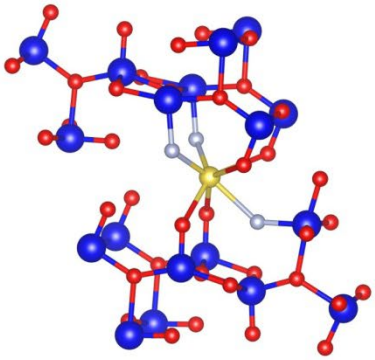

$F(1)_TF(1)_B$ 109

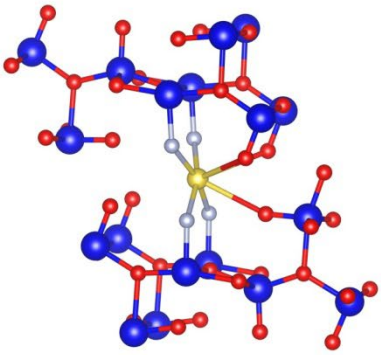

$F(1)_TF(1)''_T$ 0

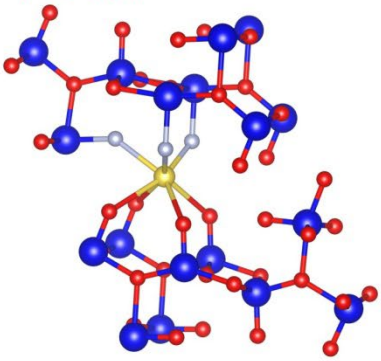

$F(1)'_TF(1)''_B$ 75

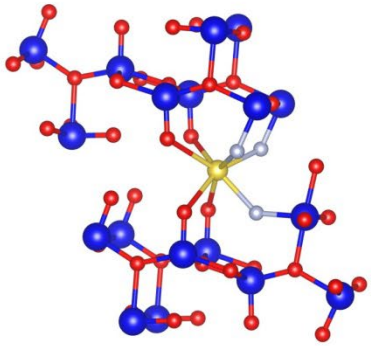

$F(1)'_TF(1)_B$ 268

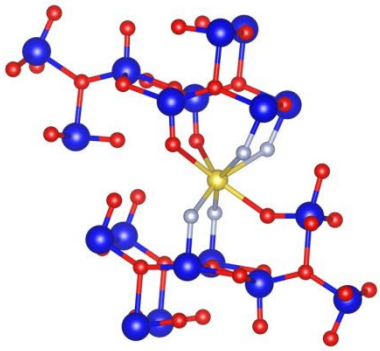

$F(1)''_BF(1)_B$ 72

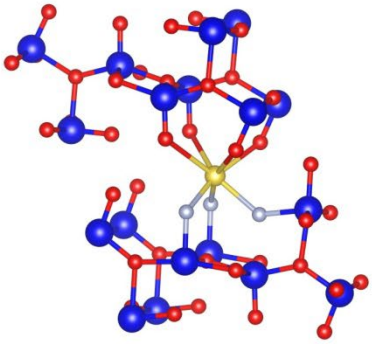

$F(1)_BF(1)'_B$ 236

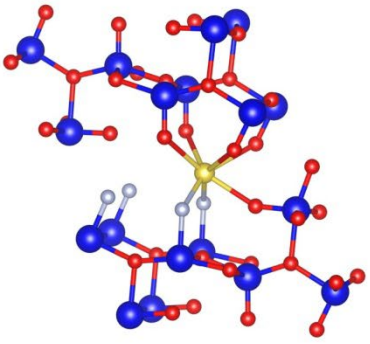

$F(1)''_TF(1)'_B$ 193

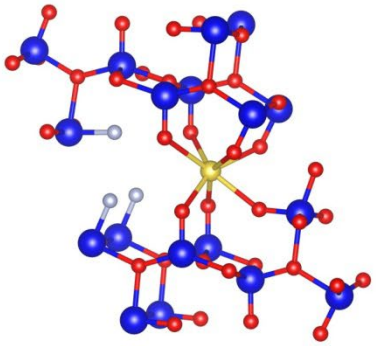

$F(1)_TF(3)'_T$ 591

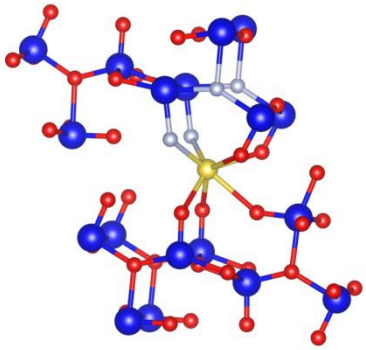

$F(3)_TF(3)_T$ 1634

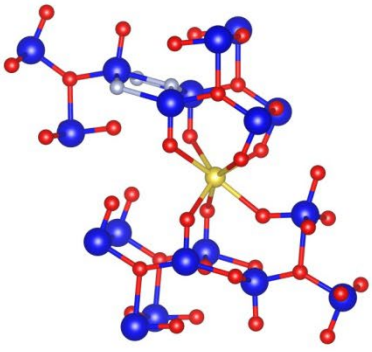

Accepted version.
Published in *Inorganic Chemistry* **2020,** *59* (22), 16361-16374.
https://doi.org/10.1021/acs.inorgchem.0c02117

Figure 5. Different structures of the bronze β-$Na_{0.33}V_2O_{4.67}F_{0.33}$ bulk unit cell with the corresponding relative energies [E_{rel} in meV] from the DFT(PBE+U)+D3 calculations. The V, O, F, and Na atoms are shown as blue, red, arctic, and yellow spheres, respectively.

The influence of the fluorine atoms on the electronic structure of the bronze β-$Na_{0.33}V_2O_5$ bulk is also presented. Fig. 4b-d shows the total and projected DOS for the three most stable bronze β-$Na_{0.33}V_2O_{4.67}F_{0.33}$ systems. The projected DOS of bronze β-$Na_{0.33}V_2O_{4.67}F_{0.33}$ shows that the F 2p states are mainly located in the bottom and middle part of VB. When we compare the DOS plot in the vicinity of the Fermi level for the doped and undoped systems, it is seen that the introduction of fluorine only slightly affects the band structures. We also found a small shift of 0.02 - 0.13 eV in the Fermi level (the dashed pink line in Fig. 4) after fluorine insertion.

Considering this small shift, little change in the redox chemistry is expected. Calculation of the potential difference between the sodium electrode and the two parent compounds (open circuit voltage) as well as the variation of voltage upon sodium intercalation have not been undertaken inasmuch as the reference sodium-free compound could not be computed as we lack structural and electronic information about the Na-free compound which could not be obtained by sodium extraction (see below).

Electrochemical sodium insertion/deinsertion properties

Fig. 6a shows the first cycle of a cell bearing either the oxide or the oxyfluoride as the active material of the positive electrode at C/20 rate (7.5 mA g^{-1}) down to 1 V vs. Na^+/Na. Insertion of Na in the oxyfluoride seems to be quite impeded when compared to the oxide. Although both compounds exhibit the same structure type, as described in the previous sections, the amount of intercalated Na in the oxide is larger under identical experimental conditions. However, the voltage

Accepted version.
Published in *Inorganic Chemistry* **2020,** *59* (22), 16361-16374.
https://doi.org/10.1021/acs.inorgchem.0c02117

profile of the first charge, shown in Fig.6a, may indicate either an oxidation mechanism different from that during reduction, as already observed in $NaFePO_4$,[63] or irreversible reduction of the oxide. In the case of the oxyfluoride, the voltage drops very fast, pointing to either a low degree of insertion or a stronger kinetic limitation due to slower ion diffusion or to the expected decrease of electronic conductivity owing to a higher bond ionicity. To rule out the influence of any irreversible transformation, galvanostatic experiments were run limiting the lower cut-off voltage to 2 V (Fig S2 of the SI). Under these conditions, the oxyfluoride presents the same behavior with fast drop of voltage ascribed to the more limited kinetics. Whatever the origin under such a polarized situation, the effect of fluorine on the intercalation voltage is not clearly discerned.

Although literature on sodium insertion on this bronze is not abundant, it appears that the amount of inserted sodium strongly relies on morphology and surface area.[32, 35] To further uncover the influence of fluorination in this material, additional electrochemical data were recorded under near-equilibrium conditions (GITT experiments) to minimize the ±IR drop contribution to the voltage.

Bach et al.[31] reported that deep discharge (down to 1.6 V vs. Na^+/Na) is responsible for a constant decrease of specific capacity. We decided to run GITT experiments in two different voltage ranges, with lower cut-off voltages below 1.6 V (1.0 V) and above 1.6 V (2.0 V), because the voltage range used in this previous report might not be useful as proper references due to kinetic limitations detected in the oxyfluoride.

Experiments run under GITT conditions (Fig 6b and 6c) reveal reversible Na insertion behavior and similar voltage profiles under thermodynamic equilibrium in both OCV - 2.0 V and OCV-1.0 V voltage ranges. Interestingly, when the systems are left to reach equilibrium with negligible polarization, the average voltage of β-$Na_{0.33}V_2O_{4.66}F_{0.33}$ is still lower than that of the oxide for the same sodium content. This is a striking feature if one considers that fluorination was made to pursue

Accepted version.
Published in *Inorganic Chemistry* **2020,** *59* (22), 16361-16374.
https://doi.org/10.1021/acs.inorgchem.0c02117

an increase in voltage. However, direct comparison of experimental voltages for oxide and oxyfluoride may not be valid inasmuch as the aliovalent O/F substitution has an influence on the oxidation state of vanadium for the same sodium content. A proper comparison reflecting the expected effect on voltage is shown in Fig. 6d that shows the quasi-equilibrium voltage profile as a function of the estimated oxidation state considering the initial sodium content and the amount of electrochemically inserted sodium. For the sake of clarity, only the wider voltage range (OCV – 1 V) is shown. It turns out that the equilibrium potential is systematically higher for the oxyfluoride during both discharge and charge processes in the whole voltage range. The potential difference is maximum, 0.6 V, for β-$Na_{0.33}V_2O_{4.66}F_{0.33}$ at the open-circuit-voltage (for which the estimated oxidation state is +4.66) and continuously decreases upon discharge. This observation can be related to the residual polarization observed even under GITT conditions and may be due to different kinetics of both electrochemical interfacial and mass diffusion processes. Note that oxide and oxyfluoride exhibit very different morphologies and particle sizes as evidenced from SEM studies (See Fig. 2b)

Accepted version.
Published in *Inorganic Chemistry* **2020,** *59* (22), 16361-16374.
https://doi.org/10.1021/acs.inorgchem.0c02117

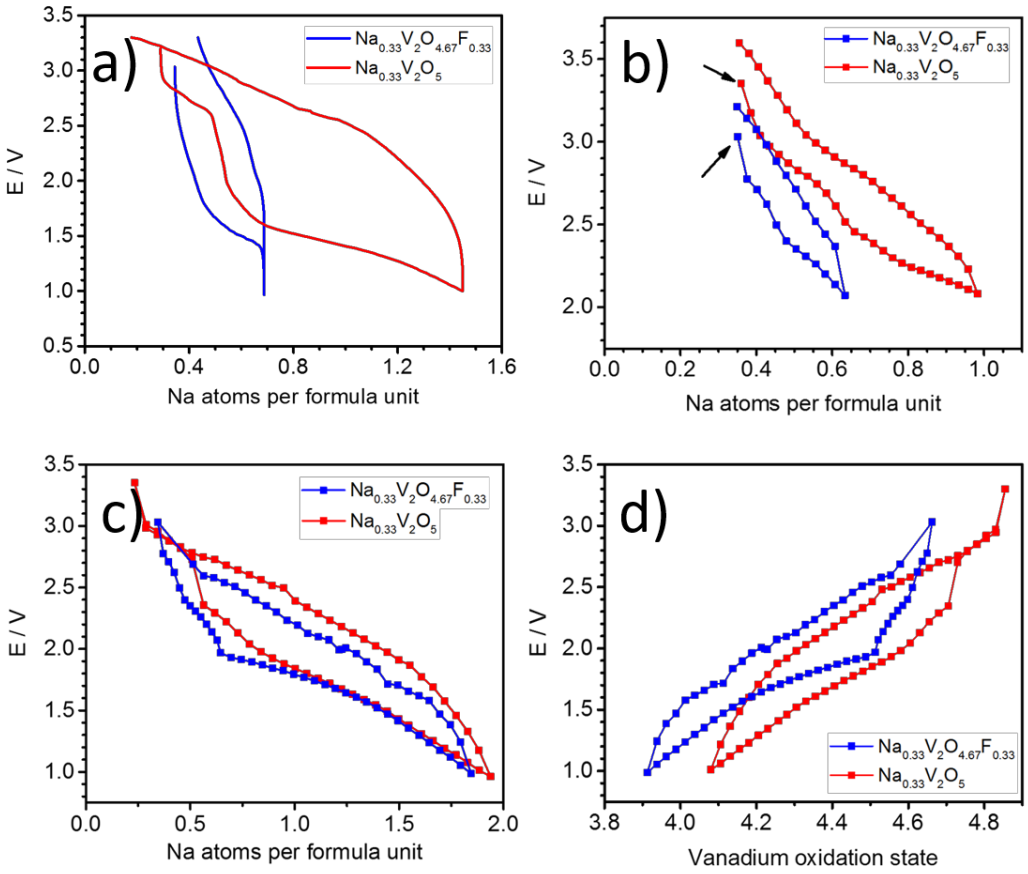

Figure 6. a) Voltage-composition profile at C/20 rate down to 1 V; Voltage-composition profile under GITT conditions in the range b) OCV - 2 V and c) OCV - 1 V; d) quasi-equilibrium voltage profile as a function of estimated vanadium oxidation state.

Electrochemical results presented herein and in previous reports[31, 64] indicate that β bronze $Na_{0.33}V_2O_5$ deserves attention as an electrode for sodium-ion batteries, inasmuch as the capacity in the OCV - 1.0 V vs. Na^+/Na voltage range, corresponding to the reaction with 1.66 Na^+/f.u., is one of the highest among sodium cathodes (ca. 245 mAh g^{-1}). The higher equilibrium voltage observed in the oxyfluoride β-$Na_{0.33}V_2O_{4.66}F_{0.33}$ anticipates a higher specific energy. However, the lower capacity owing to the lower oxidation state of vanadium in $Na_{0.33}V_2O_{4.66}F_{0.33}$ and higher

Accepted version.
Published in *Inorganic Chemistry* **2020,** *59* (22), 16361-16374.
https://doi.org/10.1021/acs.inorgchem.0c02117

polarization when cells are cycled at a constant current (for example at C/20 as shown in Fig 6a or S2) frustrates the improvement. Note that aliovalent O/F substitution reduces the initial oxidation state of V and hence the amount of sodium that can be inserted decreases. This is more clearly seen in the high voltage range, shown in Fig. 6b, where reversible insertion has been reported.[31, 33] Despite the quite open structure and available positions for extra sodium in the tunnel space, it may happen that diffusion of sodium along the tunnels of the structure or interfacial phenomena are slow. This impediment appears to be more pronounced in the oxyfluoride. However, the oxide seems to suffer from slow kinetics as well. Note that even under quasi equilibrium conditions discharge and charge curves are still separated by 200 to 400 mV. Apparently, full equilibrium has not been reached even under these relatively slow experimental conditions, and longer times are needed to accomplish the diffusion of charged sodium atoms accumulated on the surface of the cathode during each current step. Consequently, Fig S3 of SI shows that initial discharge capacity, Q_0 at C/20, decreases very rapidly with increasing current density in both samples, which behave in a similar manner.

In addition to Na insertion into the tunnel of the β bronzes, our considerations on limited kinetics also apply to the Na extraction to get β´-V_2O_5. We have not been able to fully extract sodium from the $Na_{0.33}V_2O_5$ aimed to prepare the polymorph β´-V_2O_5. Even after several treatments with NO_2BF_4 as oxidizing agent, elemental analysis of the resulting compound indicated that barely 33% of sodium content was removed, suggesting that sodium has a high stability in the bronze structure. Electrochemical oxidations of our samples under different conditions (see experimental section) were also unsuccessful. In this respect, Pereira-Ramos et al.[32] were also unable to remove sodium from β-$Na_{0.33}V_2O_5$ by electrochemical oxidation. Nevertheless, Kim et al.[33] more recently claimed that sodium can be totally extracted thanks to a favorable morphology. Interestingly, the morphology that

Accepted version.
Published in *Inorganic Chemistry* **2020,** *59* (22), 16361-16374.
https://doi.org/10.1021/acs.inorgchem.0c02117

these authors described is not very different from the one obtained in our oxide sample for which only partial extraction was achieved.

To ascertain the origin of such limitations regarding sodium extraction, we have determined the sodium diffusion coefficient of both the oxide and the oxyfluoride as well as resistances associated with sodium ion transport through the cell.

The three electrode cells used to avoid the contribution of the sodium anode to impedance response are described in the experimental section. Typical Nyquist plots obtained at x ~0.33 of a three-electrode cell bearing either $Na_{0.33}V_2O_5$ oxide or $Na_{0.33}V_2O_{4.66}F_{0.33}$ oxyfluoride as the positive electrode are shown in Fig. 7 (open circles). At high frequencies, an x-intercept is observed (Fig. 7 upper insets). At intermediate frequency values, experimental data show two depleted and overlapped semicircles for the oxide and a depleted semicircle for the oxyfluoride. In the low frequencies range, corresponding to slowest processes, the movement of sodium ions within the positive electrode produces the impedance response. In this range, just after the two depleted semicircles, there is a linear variation of -Im(Z) with the Re(Z) part of impedance in both cases.

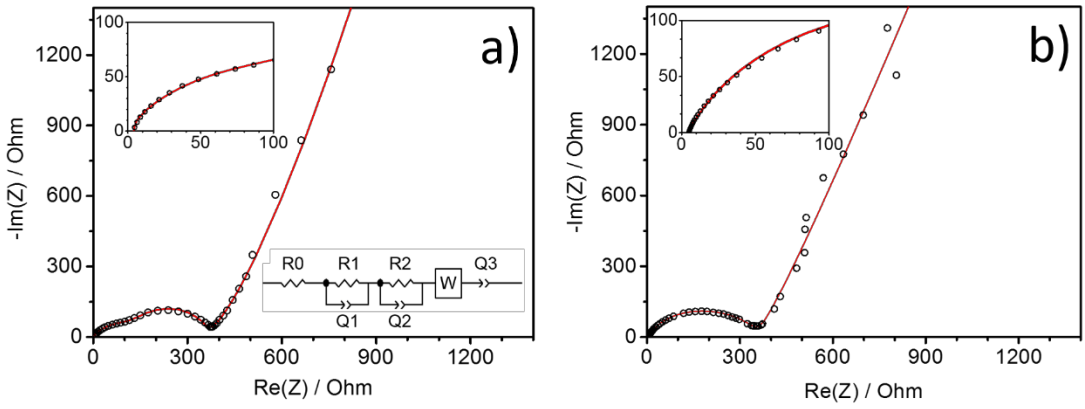

Accepted version.
Published in *Inorganic Chemistry* **2020,** *59* (22), 16361-16374.
https://doi.org/10.1021/acs.inorgchem.0c02117

Figure 7**.** Nyquist plot corresponding to impedance of the working electrode a) $Na_{0.33}V_2O_5$ electrode and b) $Na_{0.33}V_2O_{4.66}F_{0.33}$ electrode, both at x~0.33. Insets show the equivalent circuit used for both fittings and a closer view of the high frequency range.

The impedance data of both compounds has been modeled by the same equivalent circuit, associating each one of the sub-circuit elements to different physical-chemical processes. The proposed equivalent circuit is similar to that proposed by several authors.[65, 66] The x-intercept corresponds to a pure resistor (R_0) due to the cell characteristic, and it is dominated by the resistance of the transport of sodium ions through the electrolyte. The two depressed semicircles at intermediate frequencies seen in Fig. 7a are fitted with two RCPE in series where the CPE represents constant phase elements characterized by a pseudocapacitance Q instead of a pure capacitor. CPE is used when modelling impedance spectra as alternative to pure capacitors due to relaxation[67] frequency distribution. In batteries, this distribution is due to the non-ideality of the electrode surface and its interface with the electrolyte (roughness, irregularities, etc.).

The overlapping of the two semicircles indicates that the two physical phenomena ascribed to this part of the circuit model have very close relaxation frequencies. These two elements of the equivalent circuit are assigned to two different electrochemical processes that take place in the electrode-electrolyte interfaces: i) migration of sodium ions through the cathode-electrolyte interface and charge accumulation characterized by R_1 and Q_1, and ii) the charge transfer process (solvation/desolvation of sodium ions) at electrode-electrolyte interface which occurs in parallel with the electrical double layer capacitance characterized by R_2 and Q_2, respectively. In the case of the oxyfluoride, the two elements have also been used for fitting, although the two semicircles are not so clearly seen.

Accepted version.
Published in *Inorganic Chemistry* **2020,** *59* (22), 16361-16374.
https://doi.org/10.1021/acs.inorgchem.0c02117

The linear variation observed after the depressed semicircles is assigned to a Warburg impedance describing the semi-infinite diffusion process of sodium ions through the bulk of the electrode. The imaginary and real part of impedance have the same value for the ideal semi-infinite diffusion process and produce a spike with 45º in the Nyquist plot. Deviation from the ideal 45º can be associated with the charge accumulation phenomena on the electrode surface due to low diffusion into the bulk. A pseudocapacitance in series, Q_3, that describes, according to Kim et al.,[68] the charge accumulation phenomena on the electrode surface, is used to account for the deviation of the Warburg resistance. The solid line in Fig. 7 depicts the fitting of experimental data to the equivalent circuit shown in the lower inset of Fig. 7a. The fitting result for resistances and pseudocapacitances are listed in Table S6 of the SI for both oxide and oxyfluoride. Due to the strong overlapping of the two depressed semicircle elements in the oxyfluoride, no conclusions can be extracted regarding the changes in the individual processes associated with them upon partial substitution of oxygen by fluorine. However, the data clearly show that the total resistance of sodium ion migration through the cathode-electrolyte interface layer and the charge transfer process, R2+R3, are quite similar with resistances in the same order of magnitude. Note that for both compounds the total resistance is very high, explaining the large polarization observed and the large capacity loss at high current rates.

Impedance spectra showing a Warburg element can be used to characterize the kinetics of a mass diffusion process. Thus, the diffusion coefficient D_{Na+} was calculated by applying Eq.1:[69]

$$D = \left(\frac{V_m}{zFA}\right)^2 \left(\frac{dE}{dx}\right)^2 \left(\frac{1}{\sqrt{2}mA_w}\right)^2 \qquad \text{Eq. 1.}^{69}$$

Accepted version.
Published in *Inorganic Chemistry* **2020,** *59* (22), 16361-16374.
https://doi.org/10.1021/acs.inorgchem.0c02117

where V_m is the molar volume, z is the number of electrons exchanged in the redox reaction, F is the Faraday´s constant, A is the electrode specific area (determined by BET method as indicated in the experimental section), dE/dx is the local slope of the equilibrium E vs x curve at the x value where impedance measurements were made (x ca. 0.33), m is the electrode mass, and A_W is the Warburg coefficient. A_W is obtained from the Warburg region of impedance spectrum. Considering that this region can be partially overlapped by the adjacent circuit elements, the A_W value was read from the minimum of $-Im(Z)\ \omega^{1/2}$ versus ω. At this minimum, the Warburg diffusion process is the only contribution to EIS data.[70] The Warburg coefficient and the rest of parameter of Eq.1 as well as the resulting D_{Na+} are listed in Table 2.

Table 2. Values of parameters for determination of the Na diffusion coefficient in β-$Na_{0.33}V_2O_5$ and β-$Na_{0.33}V_2O_{4.66}F_{0.33}$.

$Na_{0.33}V_2O_5$					
V_m	**A**	**dE/dx**	**m**	**A_W**	**D_{Na+}**
53.37 cm^3/mol	3.01 m^2/g	-7.16 V mol	14.1 mg	6.21 Ω $s^{-1/2}$	1.13 × 10^{-12} cm^2 s^{-1}

$Na_{0.33}V_2O_{4.66}F_{0.33}$					
V_m	**A**	**dE/dx**	**m**	**A_W**	**D_{Na+}**
51.66 cm^3/mol	3.13 m^2/g	-9.92 V mol	10.2 mg	33.46 Ω $s^{-1/2}$	1.24 × 10^{-13} cm^2 s^{-1}

The sodium diffusion coefficient (D_{Na+}) of the oxide β-$Na_{0.33}V_2O_5$ is in agreement with previously reported values[71] for nanoplates β-$Na_{0.33}V_2O_5$ (3.33× 10^{-12} cm^2/s) as determined also by EIS. These authors reported an acceptably good power rate in view of the high D_{Na+}.

The other D_{Na+} of β-$Na_{0.33}V_2O_{4.66}F_{0.33}$ is one order of magnitude lower than for β-$Na_{0.33}V_2O_5$, which explains the smaller polarization and higher capacity of the latter under the same constant current (Fig. 6a and S3).

Accepted version.
Published in *Inorganic Chemistry* **2020,** *59* (22), 16361-16374.
https://doi.org/10.1021/acs.inorgchem.0c02117

Interestingly, computational results indicate that the most stable configurations of ligands around Na in β-$Na_{0.33}V_2O_{4.66}F_{0.33}$ are those that involve fluorine in its coordination polyhedron. The fact that the average Na-ligand distances are shorter in the oxyfluoride points to the same conclusion. Thus, a stronger ionic bond between Na and its ligands may be the origin of its lower D_{Na+}. We must note at this point that replacement of oxygen by fluorine may influence the diffusivity of intercalated ions in different ways since, for example, it has been claimed that doping α-MoO_3, a Mg^{2+} intercalation host [72] , with fluorine favors magnesium diffusion.[73]

However, the D_{Na+} values found neither justify the poor power rate of both oxide and oxyfluoride (Fig. S3) nor the difficulty to extract sodium. Note that sodium extraction from these two materials has only been partially achieved under our experimental conditions (see experimental section), while in the case of $NaFePO_4$ (D_{Na+} = 8.70 × 10^{-17} cm^2 s^{-1})[74] full sodium extraction is easily achieved by a relatively fast charge (at C/10 current rate). Therefore, we believe that the high value of cathode-electrolyte interface and charge transfer resistances largely contribute to the poor behavior at high current. Another important contribution to the kinetics limitation comes from the large particle size, in the range of several microns (Fig 2b), resulting from the ceramic procedures used to prepare both $Na_{0.33}V_2O_{4.66}F_{0.33}$ oxyfluoride and $Na_{0.33}V_2O_5$ oxide.

Conclusions

β-$Na_{0.33}V_2O_{4.66}F_{0.33}$ exhibits the same structure as the parent bronze β-$Na_{0.33}V_2O_5$. The partial substitution of oxygen by fluorine has little effect on the cell volume which increases only by ~ 1%. However, the sodium environment changes significantly. According to computational study, when two O atoms are replaced by two F atoms in the primitive unit cell to keep the stoichiometry, the most stable structures were found when the fluorine atoms occupy the positions of vanadyl

Accepted version.
Published in *Inorganic Chemistry* **2020,** *59* (22), 16361-16374.
https://doi.org/10.1021/acs.inorgchem.0c02117

oxygen atoms (O(1), O(1)', and O(1)'') which belong to the Na coordination polyhedron. Thus, substitution takes place mainly in the coordination sphere of Na. Little change regarding the participation of ligands in the redox chemistry is expected as the DOS plots reveal that fluorination only slightly affects the band structures with only a small shift in the Fermi level.

Interestingly, upon doping with fluorine, the average Na-O/F bond lengths determined experimentally decrease from 2.511 Å in $Na_{0.33}V_2O_5$ to 2.483 Å in $Na_{0.33}V_2O_{4.67}F_{0.33}$ (Fig. S1 of SI). The shortening of the Na-anion bond length in sodium vanadium oxyfluoride points to Na^+ surrounded with both F and O atoms. This conclusion agrees with computational results since they point to shorter sodium-anion bond lengths and simultaneously to a more fluoride-rich environment in the oxyfluoride. This different crystallochemical situation, detected by both experimental and computational methods, could affect the mobility of Na ions in β-$Na_{0.33}V_2O_{4.67}F_{0.33}$ oxyfluoride. In fact, the higher ionicity in the Na coordination sphere of β-$Na_{0.33}V_2O_{4.67}F_{0.33}$ seems to be related with a D_{Na+} one order of magnitude lower (1.24×10^{-13} cm^2 s^{-1}) than in the case of β-$Na_{0.33}V_2O_5$ (1.13×10^{-12} cm^2 s^{-1}).

Regarding the electrochemical properties, we have shown that insertion/deinsertion equilibrium potential for the same formal oxidation state of vanadium increases due to fluorination (for instance reduction of $V^{+4.3}$ occurs at 1.5 V in the oxide and at 1.75 V in the oxyfluoride). However, the capacity of $Na_{0.33}V_2O_{4.67}F_{0.33}$ at constant current is lower than in the case of β-$Na_{0.33}V_2O_5$ because of the following: i) a non-adequate morphology; ii) lower D_{Na} iii) aliovalent O/F substitution reduces the initial oxidation state of V and hence, the amount of sodium that can be inserted in the same voltage range. Decreasing D_{Na+} likely has a less significant effect because in both compounds it is high enough when compared with other state-of-the-art materials. Thus, the larger particle size and the

Accepted version.
Published in *Inorganic Chemistry* **2020,** *59* (22), 16361-16374.
https://doi.org/10.1021/acs.inorgchem.0c02117

non-acicular morphology of the oxyfluoride likely have more influence on the poorer electrochemical properties of the oxyfluoride.

Finally, optimization of the oxyfluoride material will require developing synthesis methods to obtain nanoparticles. On the other hand, high charge transfer resistances have been found in both cases. Hence, investigation of alternative electrolytes favoring charge transfer resistance and reducing resistance due to Na ion migration through the cathode-electrolyte interface will be needed.

Author Information

Corresponding Authors

flaga@ceu.es ;

j.goclon@uwb.edu.pl

Conflicts of interest

There are no conflicts of interest to declare.

Acknowledgements

We thank “Agencia Estatal de Investigación/Fondo Europeo de Desarrollo Regional” (FEDER/UE) for funding the projects MAT2016-78632-C4-1-R and PID2019-106662RB-C41. Computational resources were provided by the Interdisciplinary Centre for Mathematical and Computational Modelling (ICM), University of Warsaw, Grant number G73-11. This research was also supported in part by PLGrid Infrastructure. The computations were performed on a Prometheus supercomputer at ACC Cyfronet AGH-UST. We also thank Prof. M. J. Torralvo for BET determination. R. Córdoba wants to thank AEI and the European Social Fund/UE for the predoctoral grant BES-2017-080862.

Accepted version.
Published in *Inorganic Chemistry* **2020,** *59* (22), 16361-16374.
https://doi.org/10.1021/acs.inorgchem.0c02117

Supporting Information: Structure of bronze and bond distances. Voltage profile OCV-2 V. C-rate. Rietveld analysis of the XRD patterns. Bond valence analysis. Lattice constants and internal positions. Equivalent circuit fitting parameters

References

(1) Whittingham, M. S.; Siu, C.; Ding, J. Can Multielectron Intercalation Reactions Be the Basis of Next Generation Batteries? *Accounts Chem. Res.* **2018,** 51 (2), 258-264.
(2) Liu, R.; Liang, Z. T.; Gong, Z. L.; Yang, Y. Research Progress in Multielectron Reactions in Polyanionic Materials for Sodium-Ion Batteries. *Small Methods* **2019,** 3 (4).
(3) Song, J.; Xu, M. W.; Wang, L.; Goodenough, J. B. Exploration of $NaVOPO_4$ as a cathode for a Na-ion battery. *Chem. Commun.* **2013,** 49 (46), 5280-5285.
(4) Liang, Z. T.; Liu, R.; Xiang, Y. X.; Zhu, J. P.; Liu, X. S.; Ortiz, G. F.; Yang, Y. Electrochemical investigation of multi -electron reactions in $NaVOPO_4$ cathode for sodium -ion batteries. *Electrochim. Acta* **2020,** 351, 8.
(5) Lin, C. Y.; Duh, J. G. Porous $Li_4Ti_5O_{12}$ anode material synthesized by one-step solid state method for electrochemical properties enhancement. *J. Alloys Compd.* **2011,** 509 (8), 3680-3685.
(6) Gocheva, I. D.; Doi, T.; Okada, S.; Yamaki, J.-i. Electrochemical Properties of Trirutile-type Li_2TiF_6 as Cathode Active Material in Li-ion Batteries. *Electrochem.* **2010,** 78 (5), 471-474.
(7) Kageyama, H.; Hayashi, K.; Maeda, K.; Attfield, J. P.; Hiroi, Z.; Rondinelli, J. M.; Poeppelmeier, K. R. Expanding frontiers in materials chemistry and physics with multiple anions. *Nat. Commun.* **2018,** 9.
(8) Liang, Z. T.; Zhang, X. F.; Liu, R.; Ortiz, G. F.; Zhong, G. M.; Xiang, Y. X.; Chen, S. J.; Mi, J. X.; Wu, S. Q.; Yang, Y. New Dimorphs of $Na_5V(PO_4)_2F_2$ as an Ultrastable Cathode Material for Sodium-Ion Batteries. *ACS Appl. Energy Mater.* **2020,** 3 (1), 1181-1189.
(9) Julien, C.; Mauger, A.; Groult, H. In *Advanced Fluoride-Based Materials for Energy Conversion*; Nakajima, T., Groult, H., Ed.; Elsevier Science Bv: Amsterdam, 2015; Chapter 4.
(10) Sauvage, F.; Bodenez, V.; Vezin, H.; Albrecht, T. A.; Tarascon, J.-M.; Poeppelmeier, K. R. $Ag_4V_2O_6F_2$ (SVOF): A high silver density phase and potential new cathode material for implantable cardioverter defibrillators. *Inorg. Chem.* **2008,** 47 (19), 8464-8472.
(11) Sauvage, F.; Bodenez, V.; Tarascon, J.-M.; Poeppelmeier, K. R. Room-Temperature Synthesis Leading to Nanocrystalline $Ag_2V_4O_{11}$. *J. Am. Chem. Soc.* **2010,** 132 (19), 6778-6782.
(12) Perez-Flores, J. C.; Villamor, R.; Avila-Brande, D.; Amores, J. M. G.; Moran, E.; Kuhn, A.; Garcia-Alvarado, F. VO_2F: a new transition metal oxyfluoride with high specific capacity for Li ion batteries. *J. Mater. Chem. A* **2015,** 3 (41), 20508-20515.
(13) Cambaz, M. A.; Vinayan, B. P.; Clemens, O.; Munnangi, A. R.; Chakravadhanula, V. S. K.; Kubel, C.; Fichtner, M. Vanadium Oxyfluoride/Few-Layer Graphene Composite as a High-Performance Cathode Material for Lithium Batteries. *Inorg. Chem.* **2016,** 55 (8), 3789-3796.
(14) Chen, R. Y.; Maawad, E.; Knapp, M.; Ren, S. H.; Beran, R.; Witter, R.; Hempelmann, R. Lithiation-driven structural transition of VO_2F into disordered rock-salt Li_xVO_2F. *RSC Adv.* **2016,** 6 (69), 65112-65118.

Accepted version.
Published in *Inorganic Chemistry* **2020,** *59* (22), 16361-16374.
https://doi.org/10.1021/acs.inorgchem.0c02117

(15) Liu, H. M.; Wang, Y. G.; Li, L.; Wang, K. X.; Hosono, E.; Zhou, H. S. Facile synthesis of NaV_6O_{15} nanorods and its electrochemical behavior as cathode material in rechargeable lithium batteries. *J. Mater. Chem.* **2009,** 19 (42), 7885-7891.

(16) Venkatesh, G.; Pralong, V.; Lebedev, O. I.; Caignaert, V.; Bazin, P.; Raveau, B. Amorphous sodium vanadate $Na_{1.5+y}VO_3$, a promising matrix for reversible sodium intercalation. *Electrochem. Commun.* **2014,** 40, 100-102.

(17) Guignard, M.; Didier, C.; Darriet, J.; Bordet, P.; Elkaim, E.; Delmas, C. P2-Na_xVO_2 system as electrodes for batteries and electron-correlated materials. *Nat. Mater.* **2013,** 12 (1), 74-80.

(18) Hamani, D.; Ati, M.; Tarascon, J.-M.; Rozier, P. Na_xVO_2 as possible electrode for Na-ion batteries. *Electrochem. Commun.* **2011,** 13 (9), 938-941.

(19) Muller-Bouvet, D.; Baddour-Hadjean, R.; Tanabe, M.; Huynh, L. T. N.; Le, M. L. P.; Pereira-Ramos, J. P. Electrochemically formed alpha'-NaV_2O_5: A new sodium intercalation compound. *Electrochim. Acta* **2015,** 176, 586-593.

(20) Cordoba, R.; Kuhn, A.; Perez-Flores, J. C.; Moran, E.; Gallardo-Amores, J. M.; Garcia-Alvarado, F. Sodium insertion in high pressure beta-V_2O_5: A new high capacity cathode material for sodium ion batteries. *J. Power Sources* **2019,** 422, 42-48.

(21) de Dompablo, M.; Gallardo-Amores, J. M.; Amador, U.; Moran, E. Are high pressure materials suitable for electrochemical applications? HP-V_2O_5 as a novel electrode material for Li batteries. *Electrochem. Commun.* **2007,** 9 (6), 1305-1310.

(22) Kuhn, A.; Carlos Perez-Flores, J.; Hoelzel, M.; Baehtz, C.; Sobrados, I.; Sanz, J.; Garcia-Alvarado, F. Comprehensive investigation of the lithium insertion mechanism of the $Na_2Ti_6O_{13}$ anode material for Li-ion batteries. *J. Mater. Chem. A* **2018,** 6 (2), 443-455.

(23) Perez-Flores, J. C.; Baehtz, C.; Hoelzel, M.; Kuhn, A.; Garcia-Alvarado, F. Full structural and electrochemical characterization of $Li_2Ti_6O_{13}$ as anode for Li-ion batteries. *PCCP* **2012,** 14 (8), 2892-2899.

(24) Perez-Flores, J. C.; Baehtz, C.; Hoelzel, M.; Kuhn, A.; Garcia-Alvarado, F. $H_2Ti_6O_{13}$, a new protonated titanate prepared by Li^+/H^+ ion exchange: synthesis, crystal structure and electrochemical Li insertion properties. *RSC Adv.* **2012,** 2 (8), 3530-3540.

(25) Carlos Perez-Flores, J.; Garcia-Alvarado, F.; Hoelzel, M.; Sobrados, I.; Sanz, J.; Kuhn, A. Insight into the channel ion distribution and influence on the lithium insertion properties of hexatitanates $A_2Ti_6O_{13}$ (A = Na, Li, H) as candidates for anode materials in lithium-ion batteries. *Dalton Trans.* **2012,** 41 (48), 14633-14642.

(26) Enjalbert, R.; Galy, J. A refinement of the structure of V_2O_5. *Acta Crystallogr. Sect. C-Struct. Chem.* **1986,** 42, 1467-1469.

(27) Goclon, J.; Grybos, R.; Witko, M.; Hafner, J. Relative stability of low-index V_2O_5 surfaces: a density functional investigation. *J. Phys.: Condens. Matter* **2009,** 21 (9).

(28) Wadsley, A. D. The crystal structure of $Na_{2-X}V_6O_{15}$. *Acta Crystallogr.* **1955,** 8 (11), 695-701.

(29) Galy, J.; Darriet, J.; Casalot, A.; Goodenough, J. B. Structure of the $M_xV_2O_5$-β and $M_xV_{2-y}T_yO_5$-β phases. *J. Solid State Chem.* **1970,** 1 (3), 339-348.

(30) West, K.; Zachauchristiansen, B.; Jacobsen, T.; Skaarup, S. Sodium insertion in vanadium-oxides. *Solid State Ion.* **1988,** 28, 1128-1131.

(31) Bach, S.; Baffier, N.; Pereiraramos, J. P.; Messina, R. Electrochemical sodium intercalation in $Na_{0.33}V_2O_5$ bronze synthesized by a sol-gel process. *Solid State Ion.* **1989,** 37 (1), 41-49.

(32) Pereiraramos, J. P.; Messina, R.; Znaidi, L.; Baffier, N. Electrochemical lithium intercalation in $Na_{0.33}V_2O_5$ bronze prepared by sol-gel processes. *Solid State Ion.* **1988,** 28, 886-894.

(33) Kim, J. K.; Senthilkumar, B.; Sahgong, S. H.; Kim, J. H.; Chi, M. F.; Kim, Y. New Chemical Route for the Synthesis of beta-$Na_{0.33}V_2O_5$ and Its Fully Reversible Li Intercalation. *ACS Appl. Mater. Interfaces* **2015,** 7 (12), 7025-7032.

Accepted version.
Published in *Inorganic Chemistry* **2020,** *59* (22), 16361-16374.
https://doi.org/10.1021/acs.inorgchem.0c02117

(34) Garciaalvarado, F.; Tarascon, J. M.; Wilkens, B. Synthesis and electrochemical study of new copper vanadium bronzes and of 2 new V_2O_5 polymorphs - beta'-V_2O_5 and epsilon'-V_2O_5. *J. Electrochem. Soc.* **1992,** 139 (11), 3206-3214.
(35) Galy, J.; Carpy, A. Synthesis and crystalline structure of vanadium oxyfluoride with formula $Na_xV_2O_{5-x}F_x$ ($0 < x \leq 1$). *C. R. Seances Acad. Sci., Ser. C* **1969,** 268 (25), 2195-&.
(36) Perez-Flores, J. C.; Baehtz, C.; Kuhn, A.; Garcia-Alvarado, F. Hollandite-type TiO_2: a new negative electrode material for sodium-ion batteries. *J. Mater. Chem. A* **2014,** 2 (6), 1825-1833.
(37) Perdew, J. P.; Burke, K.; Ernzerhof, M. Generalized gradient approximation made simple. *Phys. Rev. Lett.* **1996,** 77 (18), 3865-3868.
(38) PWscf code. http://www.pwscf.org
(39) Vanderbilt, D. Soft self-consistent pseudopotentials in a generalized eigenvalue formalism. *Phys. Rev. B: Condens. Matter* **1990,** 41 (11), 7892-7895.
(40) Grimme, S.; Antony, J.; Ehrlich, S.; Krieg, H. A consistent and accurate ab initio parametrization of density functional dispersion correction (DFT-D) for the 94 elements H-Pu. *J. Chem. Phys.* **2010,** 132 (15).
(41) Anisimov, V. I.; Zaanen, J.; Andersen, O. K. Band theory and mott insulators - Hubbard-U instead of Stoner-I. *Phys. Rev. B: Condens. Matter* **1991,** 44 (3), 943-954.
(42) Liechtenstein, A. I.; Anisimov, V. I.; Zaanen, J. Density-functional theory and strong-interactions - orbital ordering in Mott-Hubbard insulators. *Phys. Rev. B: Condens. Matter* **1995,** 52 (8), R5467-R5470.
(43) Dudarev, S. L.; Botton, G. A.; Savrasov, S. Y.; Humphreys, C. J.; Sutton, A. P. Electron-energy-loss spectra and the structural stability of nickel oxide: An LSDA+U study. *Phys. Rev. B: Condens. Matter* **1998,** 57 (3), 1505-1509.
(44) Cococcioni, M.; de Gironcoli, S. Linear response approach to the calculation of the effective interaction parameters in the LDA+U method. *Phys. Rev. B: Condens. Matter* **2005,** 71 (3).
(45) Monkhorst, H. J.; Pack, J. D. Special points for Brillouin-zone integrations. *Phys. Rev. B: Condens. Matter* **1976,** 13 (12), 5188-5192.
(46) Bader, R. F. W. *Atoms in Molecules: A Quantum Theory*. New York, NY, USA, 1990.
(47) Tang, W.; Sanville, E.; Henkelman, G. A grid-based Bader analysis algorithm without lattice bias. *J. Phys.: Condens. Matter* **2009,** 21 (8).
(48) Blochl, P. E. Projector augmented-wave method. *Phys. Rev. B: Condens. Matter* **1994,** 50 (24), 17953-17979.
(49) Jovanovic, A.; Dobrota, A. S.; Rafailovic, L. D.; Mentus, S. V.; Pasti, I. A.; Johansson, B.; Skorodumova, N. V. Structural and electronic properties of V_2O_5 and their tuning by doping with 3d elements - modelling using the DFT plus U method and dispersion correction. *PCCP* **2018,** 20 (20), 13934-13943.
(50) Momma, K.; Izumi, F. VESTA 3 for three-dimensional visualization of crystal, volumetric and morphology data. *J. Appl. Crystallogr.* **2011,** 44, 1272-1276.
(51) Kokalj, A. Computer graphics and graphical user interfaces as tools in simulations of matter at the atomic scale. *Comput. Mater. Sci.* **2003,** 28 (2), 155-168.
(52) Mukainakano, Y.; Maruyama, D.; Baba, K.; Shiozaki, R. Electrode material, production method of same and lithium ion secondary battery. 2009.
(53) Brese, N. E.; Okeeffe, M. Bond-valence parameters for solids. *Acta Crystallogr. Sect. B-Struct. Commun.* **1991,** 47, 192-197.
(54) Brown, I. D.; Altermatt, D. Bond-valence parameters obtained from a systematic analysis of the inorganic crystal-structure database. *Acta Crystallogr. Sect. B-Struct. Commun.* **1985,** 41 (AUG), 244-247.
(55) Khamaganova, T. N.; Trunov, V. K. Specification of the NaV_6O_{15} structure. *Zh. Neorg. Khim.* **1989,** 34 (2), 295-298.

Accepted version.
Published in *Inorganic Chemistry* **2020,** *59* (22), 16361-16374.
https://doi.org/10.1021/acs.inorgchem.0c02117

(56) Streltsov, V. A.; Nakashima, P. N. H.; Sobolev, A. N.; Ozerov, R. P. Crystal structure study of a beta'-copper vanadium bronze, $Cu_xV_2O_5$ (x=0.63), by X-ray and convergent beam electron diffraction. *Acta Crystallogr. Sect. B-Struct. Sci.Cryst. Eng. Mat.* **2005,** 61, 17-24.

(57) Ozerov, R. P.; Streltsov, V. A.; Sobolev, A. N.; Figgis, B. N.; Volkov, V. L. Electron density in the sodium vanadium oxide bronze beta-$Na_xV_2O_5$ at 9 K. *Acta Crystallogr. Sect. B-Struct. Commun.* **2001,** 57, 244-250.

(58) Yamaura, J. I.; Isobe, M.; Yamada, H.; Yamauchi, T.; Ueda, Y. Low temperature X-ray study of beta-$A_xV_2O_5$. *J. Phys. Chem. Solids* **2002,** 63 (6-8), 957-960.

(59) Shannon, R. D. Revised effective ionic-radii and systematic studies of interatomic distances in halides and chalcogenides. *Acta Crystallogr. Sect. A* **1976,** 32 (SEP1), 751-767.

(60) Wang, D.; Liu, H.; Elliott, J. D.; Liu, L. M.; Lau, W. M. Robust vanadium pentoxide electrodes for sodium and calcium ion batteries: thermodynamic and diffusion mechanical insights. *J. Mater. Chem. A* **2016,** 4 (32), 12516-12525.

(61) Gautam, G. S.; Canepa, P.; Richards, W. D.; Malik, R.; Ceder, G. Role of Structural H_2O in Intercalation Electrodes: The Case of Mg in Nanocrystalline Xerogel-V_2O_5. *Nano Lett.* **2016,** 16 (4), 2426-2431.

(62) Watthaisong, P.; Jungthawan, S.; Hirunsit, P.; Suthirakun, S. Transport properties of electron small polarons in a V_2O_5 cathode of Li-ion batteries: a computational study. *RSC Adv.* **2019,** 9 (34), 19483-19494.

(63) Casas-Cabanas, M.; Roddatis, V. V.; Saurel, D.; Kubiak, P.; Carretero-Gonzalez, J.; Palomares, V.; Serras, P.; Rojo, T. Crystal chemistry of Na insertion/deinsertion in $FePO_4$-$NaFePO_4$. *J. Mater. Chem.* **2012,** 22 (34), 17421-17423.

(64) Wang, X. Y.; Liu, Q.; Wang, H.; Jiang, D. L.; Chang, Y. J.; Zhang, T.; Zhang, B.; Mou, H. H.; Jiang, Y. PVP-modulated synthesis of NaV_6O_{15} nanorods as cathode materials for high-capacity sodium-ion batteries. *J. Mater. Sci.* **2016,** 51 (19), 8986-8994.

(65) Chang, Y. C.; Sohn, H. J. Electrochemical impedance analysis for lithium ion intercalation into graphitized carbons. *J. Electrochem. Soc.* **2000,** 147 (1), 50-58.

(66) Dolle, M.; Orsini, F.; Gozdz, A. S.; Tarascon, J. M. Development of reliable three-electrode impedance measurements in plastic Li-ion batteries. *J. Electrochem. Soc.* **2001,** 148 (8), A851-A857.

(67) Irvine, J. T. S.; Sinclair, D. C.; West, A. R. Electroceramics: Characterization by Impedance Spectroscopy. *Adv. Mater.* **1990,** 2 (3), 132-138.

(68) Kim, D. J.; Ponraj, R.; Kannan, A. G.; Lee, H. W.; Fathi, R.; Ruffo, R.; Mari, C. M.; Kim, D. K. Diffusion behavior of sodium ions in $Na_{0.44}MnO_2$ in aqueous and non-aqueous electrolytes. *J. Power Sources* **2013,** 244, 758-763.

(69) Ho, C.; Raistrick, I. D.; Huggins, R. A. Application of AC techniques to the study of lithium diffusion in tungsten trioxide thin-films. *J. Electrochem. Soc.* **1980,** 127 (2), 343-350.

(70) Anne, H. Understanding the kinetic limitations of $NaFePO_4$ as cathode active material for Na-ion batteries. Universidad del País Vasco, 2019.

(71) Jiang, D. L.; Wang, H.; Li, G. P.; Li, G. Q.; Lan, X. Z.; Abib, M. H.; Zhang, Z. P.; Jiang, Y. Self-Combustion Synthesis and Ion Diffusion Performance of NaV_6O_{15} Nanoplates as Cathode Materials for Sodium-Ion Batteries. *J. Electrochem. Soc.* **2015,** 162 (4), A697-A703.

(72) Incorvati, J. T.; Wan, L. F.; Key, B.; Zhou, D.; Liao, C.; Fuoco, L.; Holland, M.; Wang, H.; Prendergast, D.; Poeppelmeier, K. R.; Vaughey, J. T. Reversible Magnesium Intercalation into a Layered Oxyfluoride Cathode. *Chem. Mater.* **2016,** 28 (1), 17-20.

(73) Wan, L. F.; Incorvati, J. T.; Poeppelmeier, K. R.; Prendergast, D. Building a Fast Lane for Mg Diffusion in alpha-MoO_3 by Fluorine Doping. *Chem. Mater.* **2016,** 28 (19), 6900-6908.

(74) Zhu, Y. J.; Xu, Y. H.; Liu, Y. H.; Luo, C.; Wang, C. S. Comparison of electrochemical performances of olivine $NaFePO_4$ in sodium-ion batteries and olivine $LiFePO_4$ in lithium-ion batteries. *Nanoscale* **2013,** 5 (2), 780-787.

Accepted version.
Published in *Inorganic Chemistry* **2020,** *59* (22), 16361-16374.
https://doi.org/10.1021/acs.inorgchem.0c02117

Accepted version.
Published in *Inorganic Chemistry* **2020,** *59* (22), 16361-16374.
https://doi.org/10.1021/acs.inorgchem.0c02117

Table of Contents Graphic

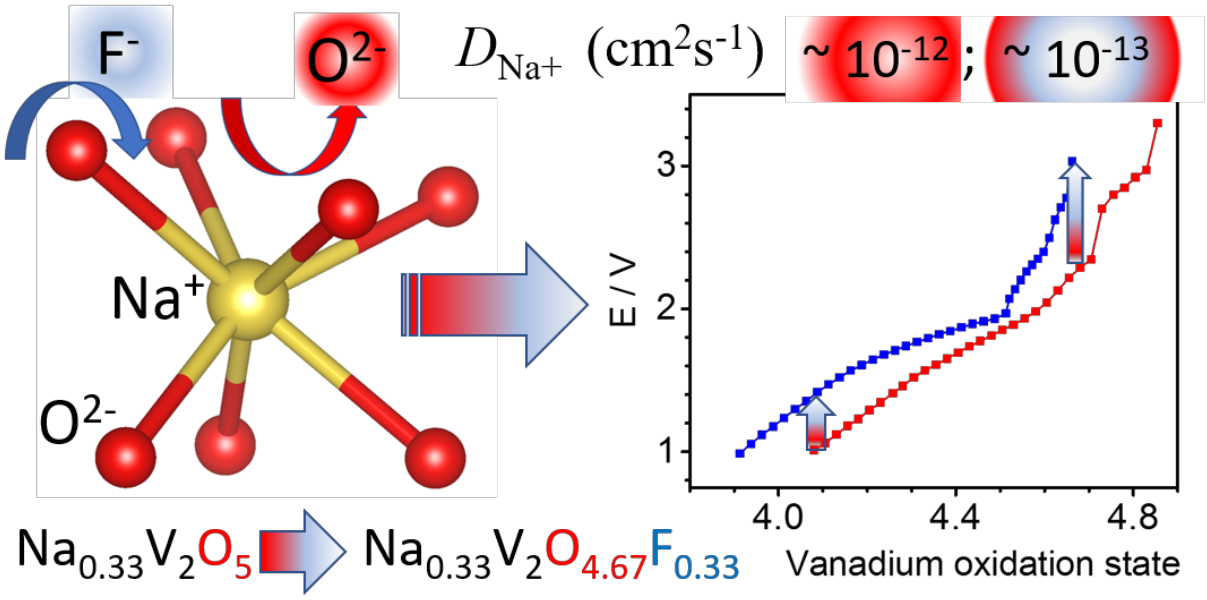

Synopsis: Partial replacement of oxide by fluoride ions takes place in the coordination sphere of Na shortening the Na-anion bond lengths. The higher ionicity in the Na coordination sphere of β-$Na_{0.33}V_2O_{4.67}F_{0.33}$ is related to a lower sodium ion diffusion coefficient, D_{Na+} than in the case of β-$Na_{0.33}V_2O_5$. Insertion equilibrium potential increases due to fluorination. Capacity is lower than for β-$Na_{0.33}V_2O_5$ due to a less adequate morphology, a lower D_{Na+}, and a lower oxidation state of vanadium.